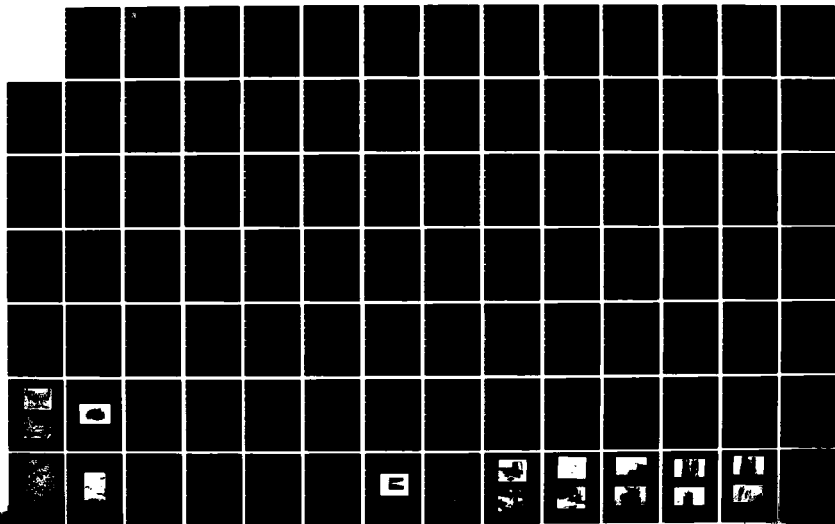


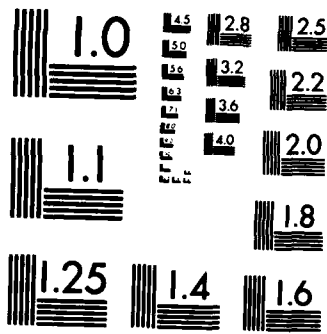
NO-R141 044

AN INVESTIGATION OF EXPERIMENTAL TECHNIQUES FOR  
OBTAINING PARTICULATE BEH. (U) AIR FORCE ROCKET  
PROPULSION LAB EDWARDS AFB CA R G CRAMER ET AL. FEB 84  
AFRPL-TR-84-014 F04611-82-X-0008 F/G 21/9.2 NL

1/2

UNCLASSIFIED





MICROCOPY RESOLUTION TEST CHART  
NATIONAL BUREAU OF STANDARDS-1963-A

2



AFRPL TR-84-014

AD:

Final Report  
for the period  
January 1982 to  
December 1983

# An Investigation of Experimental Techniques for Obtaining Particulate Behavior in Metallized Solid Propellant Combustion

February 1984

Authors:  
R. G. Cramer  
R. J. Edington  
D. E. Faber  
K. J. Graham  
B. J. Hansen  
P. J. Hickey  
L. A. Klooster  
P. J. Mellin  
J. P. Powers  
D. W. Netzer

Department of Aeronautics and  
Electrical Engineering  
Naval Postgraduate School  
Monterey, California 93943

AD-A141 044

DTIC FILE COPY

**Approved for Public Release**

Distribution unlimited. The AFRPL Technical Services Office has reviewed this report, and it is releasable to the National Technical Information Service, where it will be available to the general public, including foreign nationals.

DTIC  
ELECTE  
MAR 15 1984

*prepared for the:*

**Air Force  
Rocket Propulsion  
Laboratory**

Air Force Space Technology Center  
Space Division, Air Force Systems Command  
Edwards Air Force Base,  
California 93523

84 05 22 7

## NOTICES

When U. S. Government drawings, specifications, or other data are used for any purpose other than a definitely related Government procurement operation, the fact that the Government may have formulated, furnished, or in any way supplied the said drawings, specifications, or other data, is not to be regarded by implication or otherwise, or in any manner licensing the holder or any other person or corporation, or conveying any rights or permission to manufacture, use or sell any patented invention that may be related hereto.

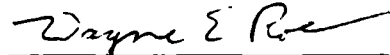
## FOREWORD

This report describes an experimental study performed at the Naval Postgraduate School under the Automatic Holographic Combustion Data Retrieval Project (JON 57300DD) under MIPR F04611-82-X-0008 and 0010.

This Final Report is approved for release and publication in accordance with the distribution statement on the cover and on the DD Form 1473.



KEVIN K. NACK, ILt, USAF  
Project Manager



WAYNE E. ROE, GM-14  
Chief, Combustion Technology Branch

FOR THE DIRECTOR



ROBERT L. GEISLER  
Chief, Propulsion Analysis Division

AFRPL -TR-84-014

AN INVESTIGATION OF EXPERIMENTAL TECHNIQUES FOR OBTAINING  
PARTICULATE BEHAVIOR IN METALLIZED SOLID PROPELLANT COMBUSTION

Authors:	R. G. Cramer	P. J. Hickey
	R. J. Edington	L. A. Klooster
	D. E. Faber	P. J. Mellin
	K. J. Graham	J. P. Powers
	B. J. Hansen	D. W. Netzer

Departments of Aeronautics and  
Electrical Engineering  
Naval Postgraduate School  
Monterey, California 93943

February 1984

Final Report for the Period January 1982 through December 1983.

APPROVED FOR PUBLIC RELEASE; DISTRIBUTION UNLIMITED

The AFRPL Technical Services Office has reviewed this report,  
and it is releasable to the National Technical Information  
Service, where it will be available to the general public,  
including foreign nationals.

Prepared for

Air Force Rocket Propulsion Laboratory  
Director of Science and Technology  
Air Force Systems Command  
Edwards AFB, California 93523

UNCLASSIFIED

SECURITY CLASSIFICATION OF THIS PAGE (When Data Entered)

RMS REPORT DOCUMENTATION PAGE		READ INSTRUCTIONS BEFORE COMPLETING FORM
1. REPORT NUMBER AFRPL-TR-84-014	2. GOVT ACCESSION NO. <b>AD A141044</b>	3. RECIPIENT'S CATALOG NUMBER
4. TITLE (and Subtitle) An Investigation of Experimental Techniques for Obtaining Particulate Behavior in Metallized Solid Propellant Combustion		5. TYPE OF REPORT & PERIOD COVERED Final
7. AUTHOR(s) R. G. Cramer, R. J. Edington, D. E. Faber, K. J. Graham, B. J. Hansen, P. J. Hickey, L. A. Klooster, P. J. Mellin, J. P. Powers, D. W. Netzer		6. PERFORMING ORG. REPORT NUMBER
9. PERFORMING ORGANIZATION NAME AND ADDRESS Departments of Aeronautics and Electrical Engineering Naval Postgraduate School Monterey, California 93943		8. CONTRACT OR GRANT NUMBER(s) F04611-82-X-0008 F04611-82-X-0010
11. CONTROLLING OFFICE NAME AND ADDRESS Air Force Rocket Propulsion Laboratory/DYC Edwards Air Force Base, California 93523		10. PROGRAM ELEMENT, PROJECT, TASK AREA & WORK UNIT NUMBERS  573000DD
14. MONITORING AGENCY NAME & ADDRESS (if different from Controlling Office)		12. REPORT DATE FEBRUARY 1984
		13. NUMBER OF PAGES 94
		18. SECURITY CLASS. (of this report) Unclassified
		18a. DECLASSIFICATION/DOWNGRADING SCHEDULE
16. DISTRIBUTION STATEMENT (of this Report)  Approved for public release; distribution unlimited.		
17. DISTRIBUTION STATEMENT (of the abstract entered in Block 20, if different from Report)  Approved for public release; distribution unlimited.		
18. SUPPLEMENTARY NOTES		
19. KEY WORDS (Continue on reverse side if necessary and identify by block number) Solid Propellants, Particulates, Optical Methods		
20. ABSTRACT (Continue on reverse side if necessary and identify by block number) A continuing investigation is being conducted to develop techniques which can be used to obtain quantitative data that can be used to relate solid rocket propellant composition and operating environment to the behavior of solid par- ticulates within the grain port and exhaust nozzle. The techniques employed are high speed motion pictures of propellant strand burners and slab burners in a cross-flow environment, SEM analysis of post-fire residue (strand, slab, and motor), determination of $D_{32}$ across the exhaust nozzle using measurements of		

DD FORM 1473  
1 JAN 73EDITION OF 1 NOV 65 IS OBSOLETE  
S/N 0102-LF-014-6601UNCLASSIFIED  
SECURITY CLASSIFICATION OF THIS PAGE (When Data Entered)

20. Abstract, continued

scattered laser light, and holograms of burning propellant strands and slabs in a cross-flow environment. In addition, work has been initiated to develop automatic data retrieval methods for obtaining particle size distributions from holograms taken of the combustion of solid propellants.

Actual particle sizes of burning aluminum particles were obtained in high speed motion pictures by using high intensity rear illumination of the burning propellants to eliminate the flame envelopes surrounding the burning particles.

Measurements of diffractively scattered light were successfully made for determination of changes in  $D_{32}$  across a solid propellant rocket motor exhaust nozzle. However, to date, propellant composition and grain geometry have significantly limited the range of obtainable data.

Two-dimensional motors have been successfully employed to obtain good quality holograms of propellant burned in a cross-flow environment. Other efforts have included reduction of speckle in the recorded hologram and optimization of techniques for minimizing excessive smoke.

A Quantimet 720 has been used in an initial effort to obtain particle size distributions from a photograph taken of a reconstructed hologram. Current efforts are directed at using a computer-controlled Quantimet 720 and a computer-controlled x-y-z translation stage to obtain particle size data directly from the reconstructed hologram.

Accession For	
NTIS GRA&I	<input checked="" type="checkbox"/>
DTIC TAB	<input type="checkbox"/>
Unannounced	<input type="checkbox"/>
Justification	
By _____	
Distribution/	
Availability Codes	
Dist	Avail and/or
	Spec



TABLE OF CONTENTS

I. INTRODUCTION . . . . . 1

II. PROPELLANTS . . . . . 3

III. COMBUSTION BOMB/HIGH SPEED MOTION PICTURES . . . . . 4

    A. Experimental Apparatus and Procedures . . . . . 4

    B. Results and Discussion . . . . . 6

    C. Conclusions . . . . . 7

IV. PARTICLE SIZING USING MEASUREMENTS OF DIFFRACTIVELY SCATTERED LIGHT . . . . . 9

    A. Introduction . . . . . 9

    B. Experimental Apparatus and Procedures . . . . . 9

    C. Results and Discussion . . . . . 15

    D. Conclusions . . . . . 17

V. HOLOGRAPHIC STUDIES USING THE TWO-DIMENSIONAL MOTOR . . . . . 19

    A. Introduction . . . . . 19

    B. Experimental Apparatus and Procedures . . . . . 20

        1. 2-D Motor . . . . . 20

        2. Laser . . . . . 23

        3. Holocamera . . . . . 24

        4. Hologram Reconstruction . . . . . 24

        5. Pre-Firing Preparation . . . . . 24

        6. Hologram Processing . . . . . 25

    C. Results and Discussion . . . . . 25

    D. Conclusions . . . . . 29

VI. AUTOMATED RETRIEVAL OF PARTICLE SIZE DATA FROM RECONSTRUCTED HOLOGRAMS . . . . . 30

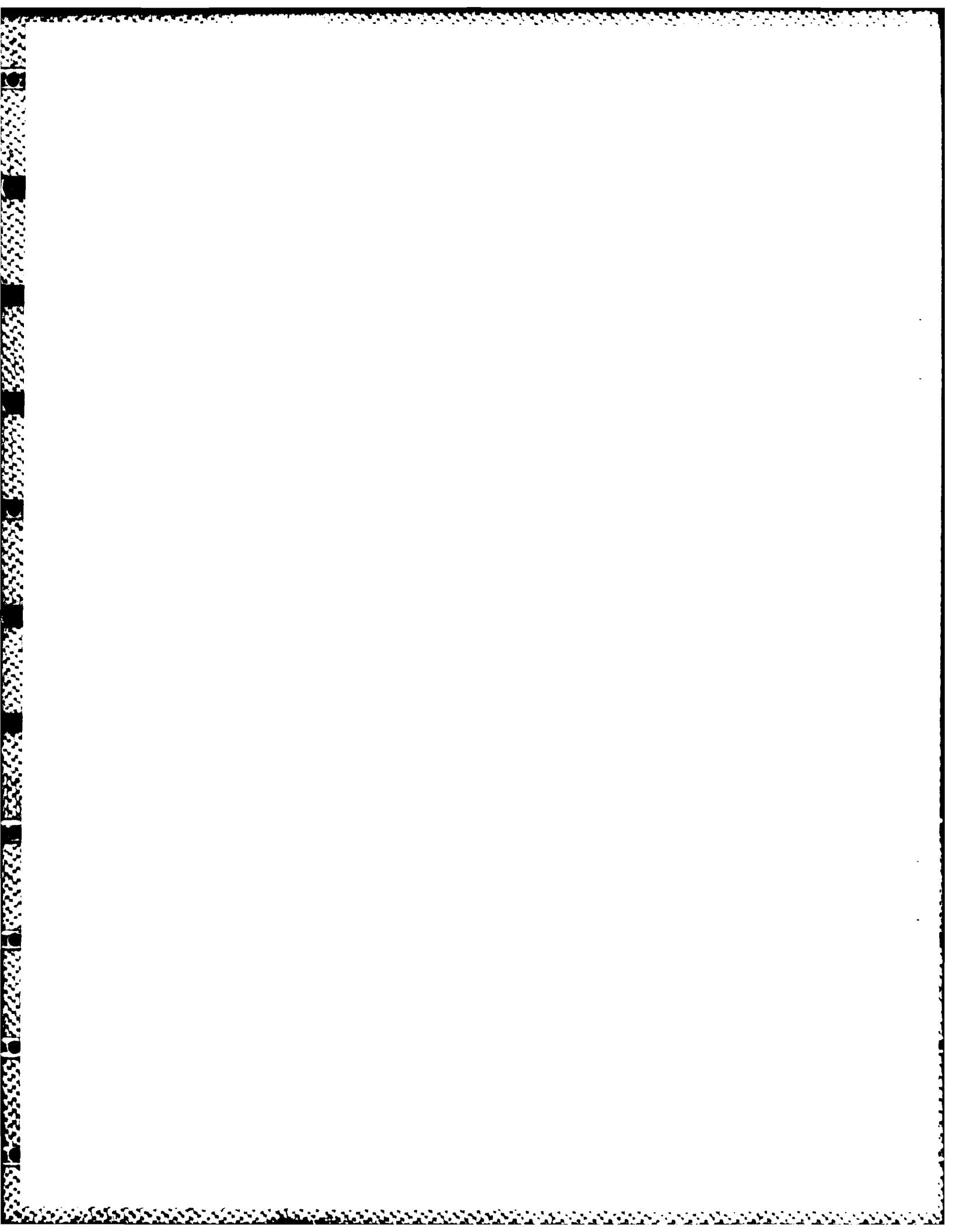
    A. Introduction . . . . . 30

B. Experimental Apparatus and Procedures . . . . .	30
1. General Description of the Quantimet 720 . . . . .	30
2. Types of Measurements Using the Quantimet 720 . . . . .	34
3. Limitations of the Quantimet 720 . . . . .	35
4. Procedure for Obtaining Measurements . . . . .	36
C. Results and Discussion . . . . .	40
1. Demonstration of Data Reduction . . . . .	40
2. Sources of Error . . . . .	41
D. Conclusions and Current Efforts . . . . .	48
1. Installation . . . . .	48
2. Testing and Operation . . . . .	48
3. Planned Efforts . . . . .	48
LIST OF FIGURES . . . . .	ix
LIST OF TABLES . . . . .	xv
LIST OF REFERENCES . . . . .	50

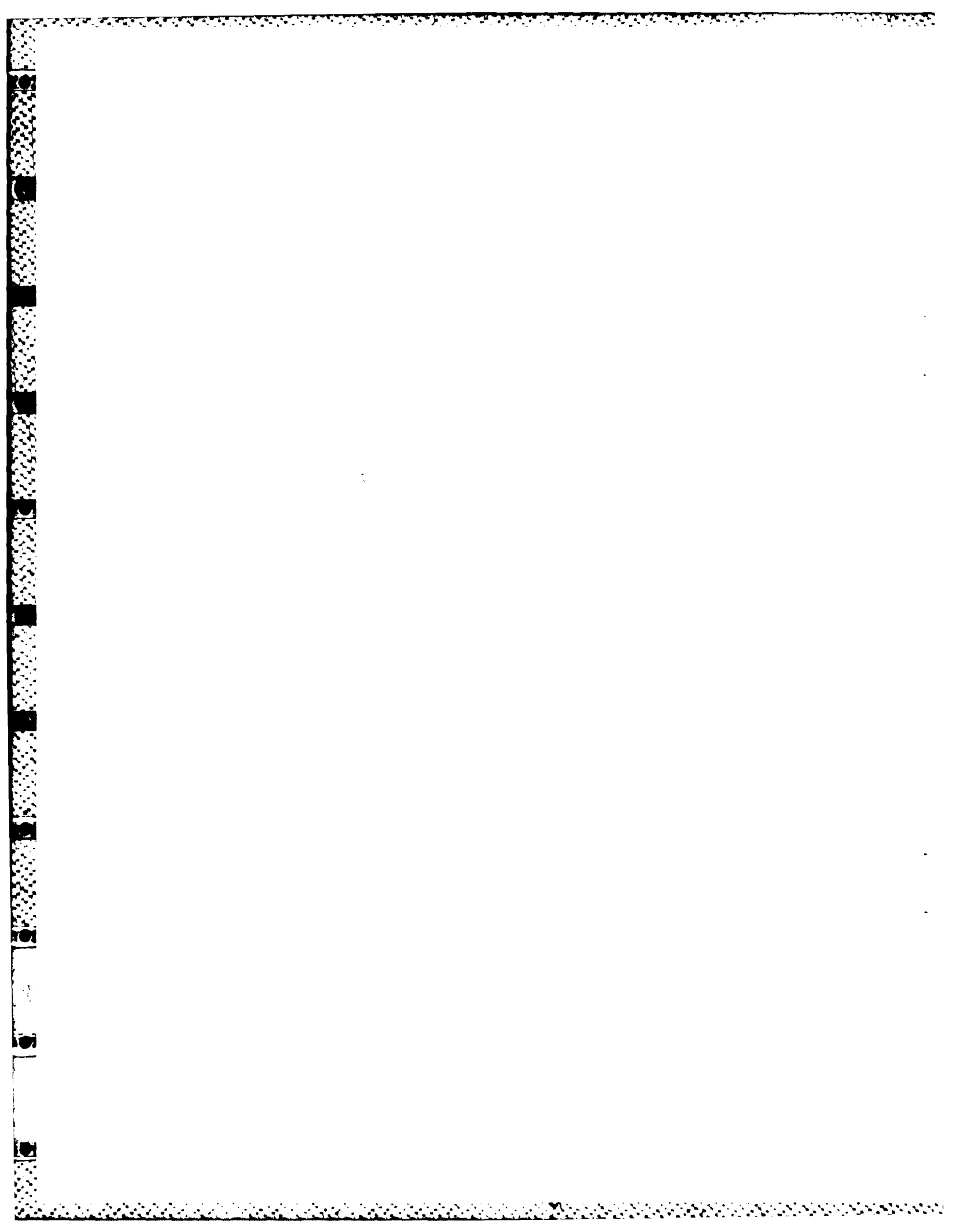
LIST OF FIGURES

1.	Schematic of Larger Combustion Bomb Showing Principal Dimensions . . . . .	52
2.	Schematic of High Pressure Combustion Bomb Showing Principal Dimensions . . . . .	53
3.	Schematic of Narrow Pass Filter Disk . . . . .	54
4.	Schematic of Combustion Bomb Apparatus . . . . .	55
5.	Photographs of Propellant WGS-6A Strands Burned at 34 atm. Pressure . . . . .	56
	(a) high speed motion picture with minimum illumination . . . . .	56
	(b) high speed motion picture with 2500 watt rear illumination . . . . .	56
	(c) reconstructed hologram . . . . .	57
6.	Schematic Diagram of Diffractively Scattered Light Apparatus . . . . .	58
7.	Schematic of Data Acquisition System for Light Scattering Measurements . . . . .	59
8.	Small Motor Construction . . . . .	60
9.	Normalized Intensity Profiles, Spherical Glass Beads . . . . .	61
10.	Normalized Intensity Profiles, 1-37 $\mu\text{m}$ Glass Beads . . . . .	62
11.	Normalized Intensity Profiles, 37-44 $\mu\text{m}$ Glass Beads . . . . .	63
12.	Normalized Intensity Profiles, 53-63 $\mu\text{m}$ Glass Beads . . . . .	64
13.	Voltage vs. Diode Number - 1 kHz Filter . . . . .	65
14.	Voltage vs. Diode Number - 3 kHz Filter . . . . .	66
15.	Example of Normalized Intensity vs. Scattering Angle Profile . . . . .	67
16.	Example of Normalized Intensity vs. Dimensionless Scattering Angle Profile . . . . .	68
17.	Normalized Intensity Profiles for $\text{Al}_2\text{O}_3$ Powder . . . . .	69
18.	SEM Photograph of Cleaned Exhaust Products . . . . .	70
19.	SEM Photograph of Uncleaned Exhaust Products . . . . .	71
20.	Initial 2-D Motor Configuration Showing Plexiglas Spacer Arrangement, Top View . . . . .	72

21. Initial 2-D Motor Configuration Showing Windows and Shutter Arrangement, Side View . . . . .	73
22. Initial 2-D Motor Configuration Showing Propellant Locations and Nitrogen Pressurization, Side View . . . . .	74
23. Propellant Slab Dimensions . . . . .	75
24. Propellant Mounted Between Glass Plates . . . . .	76
25. Schematic of 2-D Motor . . . . .	77
26. Q-Switched Pulsed Ruby Recording Laser . . . . .	78
27. Lens-Assisted Holographic System . . . . .	78
28. Holocamera Box . . . . .	79
29. Holographic Reconstruction Apparatus . . . . .	79
30. Photograph of U-80 Screw from Reconstructed Hologram . . . . .	80
31. Photograph of Reconstructed Hologram of WGS-7A Burned at 26.5 atm, 1.2 mm Thick Slide Glass . . . . .	80
32. Photograph of Reconstructed Hologram of WGS-7A Burned at 41.8 atm, 5.6 mm Thick Borosilicate Glass . . . . .	81
33. Photograph of Reconstructed Hologram of WGS-7A Burned at 34.0 atm, 5.6 mm Thick Borosilicate Glass . . . . .	81
34. Photograph of Reconstructed Hologram of WGS-6A Burned at 39.1 atm, 5.6 mm Thick Borosilicate Glass . . . . .	82
35. Photograph of Reconstructed Hologram of WGS-5A Burned at 36.4 atm, 5.6 mm Thick Borosilicate Glass . . . . .	82
36. Block Diagram of Quantimet 720, Advanced Configuration . . . . .	83
37. Block Diagram of Quantimet 720, Basic Configuration . . . . .	84
38. Block Diagram of Quantimet 720, Enhanced Basic Configuration . . . . .	85
39. Frames Available in Quantimet 720 . . . . .	86
40. Setup for Photographing Holograms . . . . .	87
41. Schematic of Reconstruction and Viewing Method (Ref. 15) . . . . .	88
42. Photograph of Reconstructed Hologram of Propellant WGS-ZrC Burned at 36 atm. . . . .	89
43. Photograph of Reconstructed Hologram of Propellant WGS-ZrC Burned at 36 atm. Detected Region . . . . .	89



44. Geometry for Calculation of Speckle Diameter . . . . .	90
45. Imaging Lens Geometry . . . . .	91
46. Speckle Size vs. Lens f-Number and Magnification . . . . .	92
47. Grey Level Map of Two Differently Illuminated, Equally sized Particles . . . . .	93
48. Semiautomatic Quantimet 720 Block Diagram . . . . .	94



LIST OF TABLES

I.	PROPELLANT COMPOSITIONS . . . . .	3
II.	DATA SUMMARY - $D_{32}$ FROM MEASUREMENTS OF SCATTERED LIGHT . . . .	16
III.	DATA SUMMARY - HOLOGRAPHIC INVESTIGATION . . . . .	28
IV.	DISTRIBUTION OF PARTICLES FROM A PLANE OF A HOLOGRAM OF PROPELLANT WGS-ZrC BURNED AT 36 ATM . . . . .	40

## I. INTRODUCTION

At the Naval Postgraduate School (NPS), a continuing investigation is being conducted to obtain quantitative data that can be used to relate solid rocket propellant composition and operating environment to the behavior of solid particulates (Al, Al<sub>2</sub>O<sub>3</sub>) within the grain port and exhaust nozzle.

These data are needed to (1) improve solid propellant performance predictive capabilities, (2) provide needed input related to ammonium perchlorate (AP)-aluminum interactions for current steady-state combustion models, and (3) provide in-motor particle size distributions which will allow more accurate predictions of damping in stability analyses. The techniques employed are high speed motion pictures of propellant strand burners and slab burners in a cross-flow environment, scanning electron microscopic (SEM) analysis of post-fire residue (strand, slab, and motor), determination of D<sub>32</sub> across the exhaust nozzle using measurements of scattered laser light, and holograms of burning propellant strands and slabs in a cross-flow environment. In addition, work has been initiated to develop automatic data retrieval methods for obtaining particle size distributions from holograms taken of the combustion of solid propellants. Once developed, these techniques/diagnostic methods could be readily employed for obtaining the needed data discussed above from a series of tests in which propellant composition, motor geometry, and operating environment are systematically varied.

This report summarizes the progress made since the results reported in Reference 1. In the initial investigation, motion picture and holographic techniques were successfully demonstrated using propellant strands burned at operating pressures of 34 and 68 atm. and with up to 15% aluminum. Fourteen  $\mu\text{m}$  resolution was obtained in the high speed motion pictures with a 1.12x

magnification (and very small depth of field) and an eleven  $\mu\text{m}$  resolution was obtained in the holograms. In addition, initial measurements of  $D_{32}$  were made using measurement of scattered laser light at the exhaust of a small rocket motor. Several needed improvements to the diagnostic techniques became evident based on the initial investigation. These were:

- (1) Use of laser light and/or high intensity white light illumination and narrow pass filters with the high speed motion pictures in order to eliminate the flame envelopes around the burning particles.
- (2) Use of photo-diode linear arrays in place of a translating photo-diode in order to improve the accuracy of the measurement of scattered laser light.
- (3) Incorporation of a second diode array at the nozzle entrance so that particulate changes across the nozzle could be measured.
- (4) Increasing the power density that reaches the holographic plate by both laser and two-dimensional motor design changes.
- (5) Initiation of the development of a system for the automatic retrieval of particulate data from holograms.

Each of the major diagnostic techniques which have been used are individually discussed in this report.

## II. PROPELLANTS

Eight specially formulated composite propellants containing varying metallic powder sizes and weight percentages were used in this investigation (Table I).

TABLE I

Propellant Composition and Metal Additive Particle Size

Propellant Designation	Binder % Weight	Oxidizer % Weight*	Metal % Weight	Mean Metal Diameter, Microns
WGS-5A	HTPB 12	AP 83	AL 5	75-88
WGS-6A	HTPB 12	AP 83	AL 5	45-62
WGS-7A	HTPB 12	AP 83	AL 5	23-37
WGS-7	HTPB 12	AP 83	AL 5	6-7
WGS-9	HTPB 12	AP 78	AL 10	23-27
WGS-10	HTPB 12	AP 73	AL 15	23-27
WGS-ZrC	HTPB 14	AP 84	ZrC 2	23, irregularly shaped
WGS-G	HTPB 14	AP 84	G 2	50x20x7, flakes

\* 65% 180  $\mu\text{m}$ /35% 26  $\mu\text{m}$

These propellants were provided by the Aerojet Solid Propulsion Company.

### III. COMBUSTION BOMB/HIGH SPEED MOTION PICTURES

#### A. EXPERIMENTAL APPARATUS AND PROCEDURES

Various techniques were utilized in order to find a good illumination method which would eliminate the flame envelopes surrounding the burning metallic agglomerates and allow accurate particle size data to be obtained.

The primary monochromatic light sources used was a Control Laser, continuous-wave (CW), argon laser, Model 902A, operating at the 488 nm line. The laser provided approximately 0.8 watts of power. Beamwidth was approximately 2mm, and required a bi-concave lens to diverge the beam to the desired width for propellant strand illumination.

Two additional light sources were used in addition to the laser light source. A SLM-1200 projector with a 1200 W tungsten filament lamp, and an Oriel 2500 W Universal Arc Lamp Source with a 2500 W Mercury/Xenon arc lamp were used. Infra-red filters were used between the white light sources and the combustion bomb windows to reduce the influence of the light sources on the combustion process.

A Hycam Model K2004E-115 high-speed, 16-mm motion picture camera was used as the recording apparatus. The Hycam is capable of operating between zero and 11,000 frames per second, with 5,000 frames per second being the highest used, and 2,500 the lowest. A RedLake Millimite TLG-4 oscillator set at 1,000 pulses per second was used to provide timing marks on the film edge on all runs.

Initially, a 7 cm extension tube was used with an Elgeet, 3 inch, f/1.9 lens to give an object distance of 6.7 cm. This placed the camera lens to within 1.0 cm of the high pressure combustion bomb window. This was the minimum working distance due to the window mounting screws, and the need to provide room for the narrow-pass filter to be placed between the lens and the

window. The obtainable resolution was 14  $\mu\text{m}$  (Reference 1). The magnification on the film was 1.90x with an effective depth of field of approximately 0.2 mm.

Because of the larger diameter of the low pressure combustion bomb used for the experiments with frontlighting, a 5 cm extension tube had to be used. This, again, put the lens at the minimum working distance possible. The 5 cm extension provided a magnification of 1.8. The effective f-stop in this configuration was 5.3, giving a depth of field of approximately 0.24 mm. Two different combustion bombs were used. One was operated to a maximum pressure of 500 psi (Figure 1) and was used when front/side illumination was required. The other bomb (Figure 2) was operated to 1500 psi and used when only rear illumination was required.

A rotating disk was used to present varying illumination (white light and 488 nm light) to the camera during a single burn. The disk was made of aluminum with a radius of 10.5 cm and a thickness of 0.58 cm. A Sargent Cone Drive Stirring Motor was used to rotate the disk at a rate of 1,740 revolutions per minute. Figure 3 presents a schematic of the disk.

Small propellant strands (10 mm high x 7 mm wide x 2 mm thick) were used in the combustion bombs.

Initially, the 0.8 watt argon laser was used as the primary monochromatic light source together with a narrow-pass laser line filter in front of the camera lens. Two illumination approaches were tried, backlighting and frontlighting. Careful examination of the films in which backlighting was used revealed that the flame envelopes surrounding the particles could be eliminated and that the true particle sizes could be seen. However, schlieren effects caused by the thermal gradients and the reasonably collimated illumination obscured much of the information that could otherwise be present

on the film. Using the argon laser for frontlighting of the propellant strand eliminated the schlieren effects but provided only limited reflected monochromatic light to the film.

The current illumination method uses three illumination sources during one test (Figure 4); 2,500 watt white light rear illumination, 1,200 watt white light side/front illumination, and 0.8 watt side/front illumination at 488 nm. With this illumination method the rotating filter disc is placed between the combustion bomb window and the camera lens. This provides alternating frames with high intensity white light illumination and filtered 488 nm illumination.

#### B. RESULTS AND DISCUSSION

In general, the use of non-diffuse laser illumination for backlighting yields unsatisfactory films from which particle size data can be readily obtained. This is due to the closely-spaced schlieren effects caused by the collimated light passing through the many thermal gradients that exist through the depth of the combustion zone. The use of diffuse monochromatic illumination has the potential for yielding good quality pictures in which the flame envelopes are eliminated through the use of a narrow pass filter. However, using low power CW (<5 watt) lasers generally does not provide enough light intensity for high speed (>2,500 pps) motion pictures when the beam is expanded sufficiently to illuminate the entire propellant strand. If the lens is fully opened the depth of field is also sacrificed.

Back illumination with high intensity (>2,500 watt) white light has been found to be generally acceptable. The intense light allows the flame light to be overpowered, while at the same time allowing the lens to be closed down to obtain good depth of field.

Figure 5 presents a set of photographs which have been printed either from 16 mm motion picture film or from 35 mm film used to record reconstructed holograms. The propellant used in all of the pictures is WGS-6A (Table I) burned in strand form at 34 atm. pressure.

Figure 5A was obtained using low power, white light, side illumination. Most of the light results from the aluminum combustion. The burning particle diameters in Figure 5A are approximately 375  $\mu\text{m}$ , whereas the mean coarse-particle diameter from collected residue (Reference 1) was approximately 58  $\mu\text{m}$ . The latter diameter is essentially the powder size cast into the propellant.

Figure 5B was obtained using 2,500 watt, white light, rear illumination. Most of the flame light has been eliminated and the "dark particles" are readily observed. The mean diameter of these particles is approximately 60  $\mu\text{m}$ , in agreement with the collected residue analysis.

For comparison purposes, Figure 5C presents a photograph taken at one depth of a reconstructed hologram. Other particles are visible at other locations within the hologram. The mean coarse particle size is approximately 55  $\mu\text{m}$ , in good agreement with both the collected residue data and the diameters in Figure 5B.

### C. CONCLUSIONS

Many investigators have taken excellent high speed motion pictures of burning solid propellant strands. A good discussion of the general technique is presented in Reference 2. Proper combination of magnification, f/stop, illumination and film speed can result in excellent motion pictures. Flame envelopes surrounding the burning metallic particles can be eliminated, resulting in true particle sizes being imaged on the film. The major

disadvantages of high speed motion pictures are the limited depth of field associated with the higher magnifications required for good resolution and the inability to view particles within the depth of field that are shielded behind other particles.

#### IV. PARTICLE SIZING USING MEASUREMENTS OF DIFFRACTIVELY SCATTERED LIGHT

##### A. INTRODUCTION

The theoretical basis, advantages and disadvantages for using measurements of diffractively scattered light to determine mean particulate diameters has been presented in Reference 1. In that initial investigation, measurements were made at the nozzle exhaust plane of a small motor using a translating, single photodiode. Subsequently, the apparatus was modified to allow simultaneous measurement of mean particle size ( $D_{32}$ ) at the entrance and exit of the exhaust nozzle. In addition, the translating single photodiode was replaced with two 1024-element linear photodiode arrays in order to improve the accuracy and speed of the measurements.

##### B. EXPERIMENTAL APPARATUS AND PROCEDURES

A schematic diagram of the optical set-up is shown in Figure 6. A schematic of the Data Acquisition System is shown in Figure 7. The optical equipment was mounted on two parallel optical benches, one for the beam passing through the exhaust and one for the beam passing through the motor at the nozzle entrance. Initially a 5 mW Helium-Neon laser was used as the light source. This was later replaced by a 10-mW Argon laser, for reasons to be discussed later. A spatial filter/beam expander located directly in front of the light source produced a uniform light beam, one centimeter in diameter. The photodiode array assemblies each consisted of a linear photodiode array, a "mother board" circuit card and an array board. Each assembly was mounted in a light-tight black box fitted with a narrow bandpass filter. Each box was mounted on two translation stages to provide vertical and horizontal degrees of freedom. The linear photodiode array was a self-scanning photodiode array, consisting of 1024 silicon photodiodes mounted in a vertical row on 25  $\mu\text{m}$

centers (EG&G RETICON G Series). The aperture width was 26  $\mu\text{m}$ . The circuits provided an integrated, sampled-and-held output. The "mother board" contained most of the circuitry, including the driver/amplifier, clock, start, and end-of-scan functions. The array board contained only the circuitry which must be located close to the array itself. The output signal was passed through a variable low-pass filter before transmission to the data acquisition system. The reading of the array was accomplished in 36 milliseconds, which corresponds to a rate of approximately 30 kHz.

The motor was cylindrical, stainless steel with a copper nozzle. The chamber was 5.08 cm in diameter and 5.08 cm deep (Figure 8). The nozzle throat diameter was .62 cm (for a chamber pressure of 52 atm). An internally burning, six-pointed star (Figure 8) was selected for the grain design in an effort to achieve a period of steady state pressure in which to take data. The grains were 2.54 cm long and 5.08 cm in diameter with a web thickness of 1.27 cm. Each grain was cut out manually from a one inch thick slab of propellant using fabricated shaped cutters. The grains were prepared for ignition by applying a thin black powder and glue mixture to the inner surface of the grain. Electrically ignited  $\text{BKNO}_3$  was discharged from the head end of the motor onto the inner surface of the grain, thus igniting the black powder, which in turn ignited the propellant. A cylindrical stainless steel tube (20 cm O.D.) was mounted at the exhaust of the motor to collect the samples of exhaust particles for evaluation using a scanning electron microscope (SEM).

Two circular windows were mounted in the walls of the motor on either side of the nozzle entrance area. The windows were recessed from the motor chamber. To keep the windows clean, nitrogen was discharged into this recessed area and evenly diffused through a sintered metal filter (Figure 8).

The accuracy of the Diffractively Scattered Light Method (References 3-12) for obtaining the mean diameter of particles was first investigated. A comparison was made between experimentally-determined normalized intensity ( $I(\theta)$ ) versus non-dimensional angle ( $\bar{\theta}$ ) profiles and the "universal" theoretical profile (Figure 9). The various profiles were first obtained using spherical glass beads of different size ranges. The individual profiles for the three size ranges of beads (1-37  $\mu\text{m}$ , 37-44  $\mu\text{m}$  and 53-63  $\mu\text{m}$ ) are shown in Figures 10-12.

The particles were suspended in water contained in a Plexiglas box (6.4 cm x 7.6 cm x 6.4 cm). Suspension was maintained using a magnetic stirrer. The first step in this calibration procedure was to obtain the zero-scattering profile, that is, the light intensity on each diode after passage through the stirred water, before particles were introduced. This is required in order to help eliminate the scattering caused by the optics and motor hardware. Next the particles were introduced and the intensity reading at each diode was again taken. Examples of intensity versus diode at 1 and 3 kHz filter settings are shown in Figures 13 and 14, respectively. The analog to digital conversion was accomplished by the data acquisition system.

After obtaining the two scattering profiles, a normalized intensity ( $I$ ) versus angle theta ( $\theta$ ) profile was determined according to the relation:

$$I = \frac{I_{\theta} - I_{\theta \text{ no particles}}}{I_{\theta=0} - I_{\theta=0 \text{ no particles}}} \quad (1)$$

where  $I_{\theta=0}$  is obtained by extrapolating the scattered light profile to the optical axis ( $\theta=0$ ) where the dominant light intensity is from transmitted light. The diode array currently measures the scattered light between angles of 0.003 radians ( $0.17^{\circ}$ ) and 0.054 radians ( $3.1^{\circ}$ ). The first diode would be

damaged by the intensity of the transmitted light if it were located on the optical axis. The first step in determining the normalized intensity was to calculate the numerator of equation (1) by subtracting the two voltages at corresponding diode numbers. The maximum difference (lower limit on diode number) computed was taken as the smallest angle where the diffractively scattered light intensity was dominant over the transmitted light intensity. An upper limit on diode number was taken near the point where  $I_{\theta} - I_{\theta \text{ no particles}}$  first became zero (Figure 14). A least squares linear fit was then made to the  $\Delta$ -voltage vs diode number data and extrapolated to obtain the denominator in equation (1) (the forward scattered light from the particles at  $\theta=0$ ).  $I$  vs.  $\theta$  could then be calculated (equation (1)). An example of the result thus produced is shown in Figure 15. At this point the relationship of  $I(\theta)$  vs.  $\bar{\theta}$  is determined using the relationship:

$$\bar{\theta} = \frac{\pi D_{32}}{\lambda} \theta \quad (2)$$

where  $D_{32}$  is the mean diameter of the particles being used in the calibration.  $I(\theta)$  vs.  $\bar{\theta}$  can then be plotted (Figure 16). An nth order polynomial curve fit was then applied to the data over a user specified range. The order of the polynomial (also user specified) may be varied from 1 to 10 depending on the appearance of the data. The range corresponded to the range of the diodes selected for determination of the  $\theta=0$  values as mentioned above. An example of the result of this process is shown in Figure 16. The results shown in Figures 9-12 for glass spheres generally agreed with those obtained with the original apparatus (Reference 1) that utilized a translating, single photodiode in that larger deviations from the universal curve occurred as  $\bar{\theta}$

was increased (beyond  $\bar{\theta}=2.5$ ). However, unlike the earlier data, agreement with the universal curve was not dependent on particle mean diameter.

Several possible causes for this lack of agreement were investigated. First, the effect of filter setting was checked. Keeping all other variables constant, data were taken with 1 kHz and 3 kHz filter settings. The resultant profiles were almost identical. Next, the effect of horizontal displacement of the array was studied. Again, keeping all other variables constant, two runs were made. The first had the focal point centered on the axis of the array. In the second, the focal point was displaced to one side, just far enough to minimize non-uniform intensity variations. Again, the results showed little difference from one another. A narrower particle suspension box was also used to decrease the depth of the field, but it likewise showed little change from the profile using the wider box. Signal-to-noise ratio and dark current were two factors which could not be completely eliminated and may contribute to the lack of agreement at higher  $\bar{\theta}$ .

Using the same procedure as discussed above,  $I(\theta)$  versus  $\bar{\theta}$  profiles were prepared for four size ranges of non-spherical  $Al_2O_3$  powder. The results are shown in Figure 17. The experimental profiles had greater slopes than the theoretical profile as they did for the spherical glass beads. However, for the  $Al_2O_3$ , the mean size affected the profile.

The particle size measuring technique was then applied to actual motor firings. Before each motor firing, calibration of the recording equipment was conducted. Proper positioning of the laser beam on the array was verified. A zero scattering profile was then recorded. The motor was fired and the scattering profile was recorded on a Visicorder oscillograph. In the same manner as previously described the normalized intensity ( $I$ ) versus angle ( $\theta$ ) was determined. At this point, either the universal profile or one of the

calibration curves can be entered at a selected value of  $I$  (or  $\theta$ , at values where the best calibrations occurred) to obtain  $\bar{\theta} = \frac{\pi D_{32}^{\theta}}{\lambda}$  and, therefore,  $D_{32}$ .

Alternatively, the ratio of  $(I_{\theta} - I_{\theta_{\text{no particles}}})$  obtained at two scattering angles can be used to obtain  $D_{32}$ . For example, if a Gaussian approximation is made to the theoretical scattering profile (Reference 13) then

$$\frac{I_2}{I_1} = \exp \left[ - \left( \frac{0.57\pi D_{32}}{\lambda} \right)^2 (\theta_2^2 - \theta_1^2) \right] \quad (3)$$

In the present investigation  $D_{32}$  values were calculated over the recorded  $\bar{\theta}$  range, using both calibration curves and the universal curve.

Residue from the motor exhaust was captured in a stainless steel collection tube. Some of it was dissolved in acetone, subjected to an ultrasonic vibrator, allowed to settle and then dried in a vacuum oven. This "cleaned" sample and an "as collected" sample were examined with SEM. Photographs are shown in Figures 18 and 19.

Considerable difficulty was encountered during the initial set-up of the computer-controlled data acquisition and data reduction procedures. When the apparatus was applied to actual motor firings several additional problems occurred.

Keeping the windows clear without affecting either motor flow or the combustion processes presented some initial difficulty. The final solution (Figure 8) consisted of a sintered metal filter to evenly diffuse the nitrogen into the window purge area and a converging nozzle to slightly accelerate the nitrogen flow into the motor. This system worked very well at all pressures investigated.

The light generated during the combustion process within the motor (but not at the nozzle exit) was found to produce a significant amount of radiation at the wavelength of the He-Ne laser ( $.6328 \mu\text{m}$ ) which was initially used as the light source. This prohibited the measurement of any scattered light from the particles. The light source was changed to an Argon laser ( $.4880 \mu\text{m}$ ) and the problem was alleviated.

The location of the laser beam in the exhaust jet was found to be critical. If directed too far to the rear of the nozzle exit it either missed the jet entirely due to the deflection of the jet or the particle number density was too low. Both problems resulted in a particle scattering profile that was nearly identical to the zero particle scattering profile. In the current experiments the beam was located three inches to the rear of the nozzle exit.

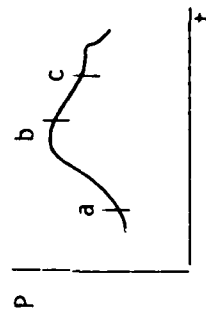
### C. RESULTS AND DISCUSSION

The tests conducted are summarized in Table II. The first series of tests were conducted at 53 atm. There were two significant results: (1) there was insufficient light through the motor to get a scattering profile; (2) the measured  $D_{32}$  in the exhaust was large ( $30\text{-}50 \mu\text{m}$ ). The photographs in Figures 18 and 19 show that the apparent reason for this large  $D_{32}$  was the presence of a small number of large irregularly shaped agglomerates, which are not Al or  $\text{Al}_2\text{O}_3$  (the latter were typically  $0.5\text{-}5 \mu\text{m}$  spheres). These agglomerates were most probably inhibitor or binder char. Their influence was significant, as even a very few large particles greatly increase the measured  $D_{32}$ . The sensitivity of the technique to irregularly-shaped particles had already been demonstrated during the calibration using  $\text{Al}_2\text{O}_3$  powder. Repeated tests resulted in different  $D_{32}$  at the nozzle exhaust, apparently from different sizes of char agglomerates at the time the diode scan was made.

TABLE II: DATA SUMMARY

Propellant contained 2% by weight of Al (40  $\mu\text{m}$ )

Run	1	2	3	4	4a (Nozzle Entrance)	5	6*
Maximum Pressure (atm)	53	53	38	38	38	34	31
Readings Taken (atm) (see fig. below)	52 (b)	52 (b)	27 (a)	37 (b)	37 (b)	32 (c)	28 (c)
D32 Average, Universal Curve ( $\mu\text{m}$ )	52	39	24	37	16	56	16
D32 Average, Calibration Curve Comparison ( $\mu\text{m}$ )**	38 m	30 m	20 s	30 s	12 s	40 $\lambda$	13 s



(Sample pressure-time trace showing points where data was taken)

\*End-burning grain

\*\*s--small particle calib.  
 m--medium particle calib.  
 $\lambda$ --large particle calib.

Figure 9

The tests made at approximately 38 atm (runs 3,4 and 5, Table II) were made to determine (1) if the size of the exhaust char agglomerates were sensitive to combustion pressure, and (2) if the lower chamber pressure would permit measurement of scattered light through the motor. In addition, repeated runs were made to acquire the diode data at different times during the run to determine whether the data was significantly time-dependent. It was found that data could be obtained through the motor. Comparisons with the universal curve and the small glass bead calibration curve yielded reasonable values for  $D_{32}$  of 16 and 12  $\mu\text{m}$ , respectively. It was further determined that  $D_{32}$  measured at the nozzle exit was sensitive to burn time, as shown by the increasing values of  $D_{32}$  with increased time. Since the spherical Al/Al<sub>2</sub>O<sub>3</sub> particles (in the collected exhaust products) were still in the 0.5 to 5  $\mu\text{m}$  size range, the change in measured  $D_{32}$  was apparently due to changes in char agglomerate size during the run.

In run 6, an end-burning grain was used in an attempt to reduce or eliminate the large char agglomerates. The results were: (1) a significant reduction in measured  $D_{32}$  (however, it was still larger than the Al/Al<sub>2</sub>O<sub>3</sub> spheres), and (2) the larger optical path with particles (increased optical density) precluded the measurement of any scattering data through the motor cavity.

#### D. CONCLUSIONS

Measurements of diffractively scattered light can be used for the determination of changes in  $D_{32}$  across a solid propellant rocket motor exhaust nozzle. However, propellant composition and grain geometry appear to significantly limit the range of obtainable data.

Two approaches are currently being used to improve this diagnostic technique; improvement of the propellant and improvement of the instrumentation. Rather than one sweep of the diode arrays during one firing, seven will be accomplished. This is being made possible by expanding the memory of the multiprogrammer in the data acquisition system and by utilization of the HP9836S computer. This should result in a more statistically valid data sample. The Air Force Rocket Propulsion Laboratory (AFRPL), is currently fabricating GAP propellants to replace the HTPB propellants which are currently being used. This may result in "cleaner" exhaust products and improve the accuracy of the measured particle sizes. Successful demonstration of the technique using the GAP (or other "clean" propellants) propellants could then be followed with a series of needed tests in which the effects of chamber pressure, nozzle geometry, and propellant ingredients (over limited ranges) are determined.

## V. HOLOGRAPHIC STUDIES USING THE TWO-DIMENSIONAL MOTOR

### A. INTRODUCTION

The objective of the current effort was to continue the development of a simple, reliable method for holographic observation of particle behavior in an environment similar to that found in the port of an actual solid rocket motor. To duplicate motor cross-flow conditions, a 2-D motor which used horizontally opposed slabs was selected.

For the exposed scene (the chamber volume illuminated by the laser beam), a hologram provides both amplitude (as in conventional photography) and phase information. The latter characteristic enables a 3-D image to be reconstructed so that particle behavior in the entire depth of field of the combustion chamber may be recorded. The flame envelope surrounding the burning particles can be eliminated with a narrow pass filter located between the scene and the holographic plate.

Single pulsed holography provides a means for effectively stopping the motion. However, it only provides information during a single instant of time. Smoke generation (i.e., small  $Al_2O_3$  and binder products, etc.) during the combustion process presents a major obstacle to obtaining good holograms, and consists of two distinct but related problems.

The first is that a laser can only penetrate a finite amount of smoke, and the second involves the required scene beam to reference beam illumination ratio. To obtain a high-quality hologram, the illumination ratio reaching the holographic plate should be between 5-10:1. Test-to-test variation of the amount of smoke in the beam path can significantly affect this ratio. To achieve an optimum combination of low levels of combustion chamber smoke and

well-developed burning of the propellant slabs requires experimental determination of the most suitable slab dimensions and the optimum time for taking the hologram during the burn.

## B. EXPERIMENTAL APPARATUS AND PROCEDURES

### 1. 2-D Motor

The two-dimensional motor was designed for two opposed, end-inhibited propellant slabs. A 8.9 mm diameter, high-quality glass window port was positioned where the laser beam entered the motor. The glass window port through which the laser beam exited the motor was enlarged to 18.5 mm (vs. that used in Reference 1) in diameter. This increased the laser power density incident on the photographic plate, facilitating exposures through a more opaque chamber medium. These glass windows were also moved as close as possible (given the current motor configuration) to the propellant to minimize the combustion chamber free volume, and to minimize the flow-disturbing effects produced as the window-protecting shutters were retracted.

Initially, the windows were centered at the lengthwise midpoint and inboard edge of the largest propellant slab. The smallest propellant slab was out of view of the smaller window port to facilitate maximum viewing of the combustion chamber volume.

A Plexiglas spacer was mounted on each window shutter block as shown in Figure 20. The spacers were shimmed during motor assembly to insure that both sides of the propellant slabs were in physical contact with Plexiglas. This reduced the possibility of uncontrolled side burning, kept chamber free volume to a minimum, and facilitated a cross-flow environment.

Retractable shutters protected the glass windows prior to laser activation and were retracted just prior to laser firing. The nitrogen purge

system was modified (Figure 21) to direct nitrogen across each window throughout the firing/hologram recording sequence.

The ignition method was also modified to eliminate the need for black powder as an igniter (Figure 22). A time-delay was activated at ignition initiation. At the expiration of the time delay the spring-loaded shutters were released. The rising shutters in turn tripped a microswitch, which triggered the holocamera shutter and fired the laser simultaneously. A photodiode was added to the laser system to sense laser firing in order to mark the precise time of laser activation on the pressure-time plot.

The burning propellant slabs produced insufficient pressure to pressurize the combustion chamber to the desired 34 atm. The chamber mounted above the combustion chamber (Figure 22) was pressurized with nitrogen and the burning propellant slabs provided the remaining pressure. In the opposed slab configuration, the propellant provided approximately fourteen percent of the desired steady-state pressure. The majority of the chamber pressurization was provided by the nitrogen introduced downstream of the propellant. Use of the upper chamber reduced the tendency of the pressurizing nitrogen to recirculate into the combustion region.

A 0-80 screw was mounted outside the large exit window in the scene beam path and was used to provide a scale for particulate sizing in the reconstructed hologram.

This initial investigation resulted in the development of a technique for obtaining good quality holograms of burning solid propellant in a two-dimensional motor with smokeless metal additives and with aluminum additives which used powder sizes greater than approximately 23 microns and additive mass contents of five percent or less by weight.

The techniques developed provided a greater range of data and more consistent runs than were possible with the original apparatus (Reference 1). However, shutter retraction noticeably disturbed the flow as evidenced by (1) the location of many of the particulates in the reconstructed hologram nearer the large exit window and not between the burning propellant slabs as would be expected under steady-state, cross-flow conditions, and (2) a small pressure disturbance following shutter retraction.

The first attempt to further improve the 2-D motor construction procedures consisted of bonding the propellant slabs between two pieces of Plexiglas. In addition, a very small hole (3.2 mm in diameter) was included through which the laser beam could pass without interference with the Plexiglas. It was hoped that by bonding the propellant to the Plexiglas that erratic burning would be minimized when using minimum amounts of inhibitor. The small holes were also used to minimize the disturbance created when the window protection shutters were raised just before laser firing.

Initial tests indicated that the erratic burning problem was eliminated. However, the 2-D motor flow was still strongly influenced by the side hole/window shutters.

A change was then made from Plexiglas to glass side plates because the latter did not pit and erode nearly as much as the former. Consequently, a hole through the glass plates was not necessary. Eliminating the hole provided a smooth gas flow along the length of the slab and also eliminated the need for window shutters, since the smoke and by-products no longer vented directly onto the optical windows.

This design used General Electric silicone rubber (RTV-106-Red, High Temperature) filler to form the seal around the propellant and the igniter. The RTV used as an end-inhibitor and side-inhibitor also bonded the glass to the propellant slabs. Propellant measurements are shown in Figure 23 and an assembled motor is shown in Figure 24. Propellant thickness was varied from 0.75 mm to 3 mm.

When the glass sides were used, the retractable shutters, the solenoid and the microswitch were all removed from the combustion bomb (Figure 25). Laser firing, previously initiated by microswitch closure, was accomplished after a specified time delay from ignition. Removal of the shutter apparatus significantly reduced the set-up time and significantly increased the reliability of the system.

## 2. Laser

The laser system used was a pulsed ruby laser built by TRW, Inc. under contract to the Air Force Rocket Propulsion Laboratory. It is described in Reference 14. The system is composed of a Q-switched oscillator, ruby amplifier, beam expanding telescope, alignment autocollimator, low-power helium-neon pointing laser, coolant system and pump, capacitor bank and associated power supplies. The wavelength was 0.6943 microns and the output beam diameter was approximately 3.2 cm. A one-joule pulse with a pulse length of 50 nanoseconds was used throughout this investigation. The laser system is shown in Figures 26 and 27.

### 3. Holocamera

The holocamera, also designed by TRW, Inc., is completely described in Reference 15. It was used to expose the holographic plate during the recording process and to support the plate during the reconstruction process. All holograms were constructed using diffuse illumination in order to minimize the schlieren effects produced by the burning propellant/aluminum particles. AGFA-GEVAERT 8E75 HD holographic plates were used to record the lens assisted holograms. The plate holding apparatus and assisting lenses are shown in Figure 28.

### 4. Hologram Reconstruction

During image reconstruction, the developed holographic plate was reattached to the plate holder and returned to the removable holocamera box. Rear illumination was provided by a Spectra Physics model 165-11 krypton-ion CW gas laser, at an angle of approximately  $60^\circ$  with the plate normal, shown in Figure 29. Output was one watt at a wavelength of 0.6471 microns. A variable power microscope was used to directly view the hologram. In order to minimize speckle, the reconstructed image was positioned on a rotating mylar disc. The latter was located at the focal point of the observation microscope. Photographs of the reconstructed scene were made using a 35 mm camera mounted to the microscope eyepiece.

### 5. Pre-Firing Preparation

The propellant was roughly cut to slightly oversized dimensions, then hand sanded to the desired size. RTV was applied to the sides of the propellant slabs to act as an inhibitor and to bond the propellant to the side plates.

After attachment to the support blocks, the motor was inserted into the combustion bomb and the nichrome ignition wire was soldered to the ignition wire which exited the bottom of the combustion bomb.

#### 6. Hologram Processing

The exposed holographic plate was removed from the holocamera in a darkroom and developed as follows:

- (1) Immersed in Kodak D-19 developer for 90 to 210 seconds and inspected periodically under a Kodak safelight.
- (2) When a satisfactory opacity was obtained, the plate was immersed in Kodak "Stop Bath" for 30 seconds, then rinsed in fresh water.
- (3) Kodak "Hypo-fix" was used to set the image. Processing time was 5-7 minutes.
- (4) Fresh water rinse for 10-15 minutes.
- (5) Immerse in Kodak "Photo-Flo" for one minute.
- (6) Air dry for 2-3 hours.

#### C. RESULTS AND DISCUSSION

The glass side plates almost always cracked during a test. However, high-speed color motion pictures of the burning motor showed that the cracking usually occurred at the end of the burn, upon cooling. With glass sides, the major problems were combustion product deposits on the inner surface and/or excessive smoke created when the propellant slabs were too thick. Solutions investigated were (1) a thicker coating of RTV (inhibitor) between the propellant and the glass (this provided better thermal protection for the glass but more inhibitor char), (2) different glass thicknesses, (3) a smaller piece of propellant as the igniter, (4) inhibiting some of the igniter surfaces to produce a slower pressure/temperature rise and (5) the use of borosilicate glass.

Initially, 1.2 mm thick glass microscope slides were used and yielded excellent results with low pressure and very thin propellant slabs, despite the presence of cracks.

Ordinary window pane glass of 4 mm or 5.6 mm thickness was used next. These tests were not successful because of what appeared to be too short a time interval between fully developed slab burning and the onset of glass cracking.

With the introduction of borosilicate glass, cracking became less of a problem. Rather than a random crack pattern which completely covered the area between the slabs, a single crack would often run the length of the glass, following the pre-ignition shape of the propellant surface.

Regardless of when cracking occurred, it did not degrade the quality of the hologram. Possible melting or heat-induced distortion of the inner surface of the glass, however, may have degraded hologram quality. Post-burn examination of all borosilicate motors revealed extensive areas of melted or distorted glass. Despite the drawbacks of borosilicate, it enabled excellent holograms to be obtained.

Figure 30 is a photograph of a reconstructed hologram which contained the 0-80 screw used for a particle sizing reference. Figures 31 through 35 are photographs of the reconstructed holograms of burning propellant. Table III summarizes the test conditions and results.

Several observations can be made from the results concerning the present technique for obtaining holograms in the cross-flow environment. Thin ( $\approx 1.0$  mm) propellant slabs and low pressure ( $\lesssim 27$  atm) allow good quality holograms to be obtained through much of the burn if glass-cracking is not severe. Holograms can be obtained at higher pressures ( $> 34$  atm) and with

thicker propellant slabs ( $\approx 2$  mm) if the laser is fired very soon after steady-state burning is achieved. The smaller the aluminum powder size in the propellant, for a given mass loading, the more difficult it is to obtain a hologram. This is due to the higher number density of particles and more uniformly distributed smoke/very small particles.

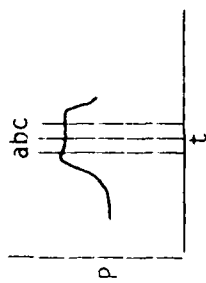


TABLE III  
DATA SUMMARY - HOLOGRAPHIC INVESTIGATION

Propellant	Pressure (atm)	Time Delay*	Propellant Thickness (mm)	Casing Material and Thickness (mm)	Hologram Figure Number	Remarks
WGS-7A	27	a	0.9	Slide Glass 1.2	31	Excellent hologram. Propellant burning.
WGS-7A	42	a	1.3	Borosilicate 5.6	32	Excellent hologram. Very early in the burn.
WGS-7A	34	a	2.0	Borosilicate 5.6	33	Excellent hologram. Early in the burn.
WGS-7A	40	c	1.8	Borosilicate 5.6	none	No hologram. Too much smoke.
WGS-6A	39	a	1.8	Borosilicate 5.6	34	Excellent hologram. Early in the burn.
WGS-5A	36	c	1.8	Borosilicate 5.6	35	Fair hologram. Much smoke, limited field of view.

\*See Pressure/Time Graph Above.

#### D. CONCLUSIONS

The use of glass side plates on the 2-D motors has allowed good quality holograms to be obtained of propellants burned in a cross-flow environment. To date, pressures have been limited to approximately 41 atm and propellant slab thickness to 2 mm. For higher pressures and smaller aluminum sizes it will probably be necessary to use thin ( $\approx 1.0\text{mm}$ ) slabs and minimum inhibitor in order to minimize smoke.

The use of glass sides also eliminated the need for combustion bomb window shutters and greatly simplified the required combustion bomb. A new, more simply constructed bomb is currently being fabricated in order to minimize motor preparation time.

## VI. AUTOMATED RETRIEVAL OF PARTICLE SIZE DATA FROM RECONSTRUCTED HOLOGRAMS

### A. INTRODUCTION

Automatic retrieval of particulate diameter data from reconstructed holograms is necessary if meaningful amounts of needed data are to be realized in a reasonable time period. Various techniques have been suggested that range from complete digitization to man-in-the-loop optical methods. A reasonable near-term solution appears to be a combination of both optical and digital methods. Klein (Ref. 16) has provided a limited demonstration of one such method, based upon the Quantimet 720 Image Analyzer.

The end goal of the NPS effort is to be able to obtain particulate diameter data from a given hologram using a reasonable amount of man-hours/computer time. Some form of image processing with a man-in-the-loop may provide a more realistic method than completely automated methods.

The NPS effort is based upon the Quantimet 720, used in conjunction with holographic reconstruction with a 1-watt krypton laser. The effort was initiated in mid-FY'83. The initial work has been directed at obtaining particle size data from a photograph taken at one location within a reconstructed hologram. Subsequent work will be directed at speckle suppression methods and obtaining data directly from traverses through the reconstructed hologram.

### B. EXPERIMENTAL APPARATUS AND PROCEDURES

#### 1. General Description of Quantimet 720

The Quantimet 720 is a general purpose television-type image analyzer that is capable of shape recognition and various physical measurements of objects by distinguishing differences in grey levels. The system was designed using a modular concept where additional capabilities can be gained by adding

modules. When used or configured as a Basic Quantimet 720, the operator must provide all control and direct all operations. In the Advanced Mode a computer is used as the controller where all operations are programmed from prior experience. The Quantimet 720 at NPS contains the necessary modules to be operated in the advanced mode but is currently being utilized in the enhanced basic mode.

Figure 36 is a block diagram of the components and shows the flow of data within a 720 configured in the Advanced Mode. The scanner sends a video signal of the sample on the epidiastope to the System Control Module where it is digitized and sent to the Variable Frame and Scale Module. The variable Frame and Scale Module, when activated, varies the blank frame size and sends the altered or standard blank frame signal forward to the 1-D Auto Detector. Here, data in the field of view (Live Frame) are differentiated by grey level. Only the isolated or highlighted data are sent to other modules to be further tested. The Light Pen can be used to isolate features for measurements. When activated, it will only allow data from the feature it is pointed at to be passed on to the other modules. The Frame Smasher is generally bypassed. The Standard Analyzer can be used to obtain measurements such as area, or it can be used to eliminate all objects greater than or less than a set chord size and pass that data to the Function Computer. The Function Computer and Classifier Collector can either provide field data or perform another test to further isolate particles for obtaining feature data. The Control Interface and FIFI provide the interface between the 720 and the computer controller. By using the Controller, image processing can be automated with little operator interaction, and it becomes possible to store a large amount of data on mass storage devices. Automation allows one to make a large number of measurements rapidly and accurately to provide sufficient data for statistical analysis.

Figure 37 is the block diagram of a 720 in the basic mode. In this configuration only field data is available; the highlighted data can be subjected to only one logic test and the operator controls all operations. In the enhanced basic mode, feature data is available and data can be subjected to two logical tests. The enhanced basic mode block diagram is shown in Figure 38.

The capabilities and operation of the modules are described in the Quantimet 720 Instruction Manual (Ref. 17).

The Quantimet 720 performs all functions within defined frames. The first frame is the image field or video frame which is the area shown on the Display, 704 by 896 pixels. The System Control Module works within that frame and outputs either Standard Big Frame, 688 by 880 pixels, or Standard Small Frame, 625 by 800 pixels, depending on the option wired. Whichever option is selected is defined as Blank Frame, the area where all detection takes place. Blank Frame, or the detection area, is usually wired as Standard Big Frame. Within it another frame is defined, the Live Frame. All computations, i.e., measurements of area, intercept, perimeter etc., take place within this frame. The Live Frame can be varied to any value by the Variable Frame & Scale Module, but is usually dimensioned as the Standard Small Frame, the default value. Between the Live Frame is the Guard Region. Figure 39 shows all frames and their locations.

The Quantimet 720 uses the pixel or picture point as its standard unit of measurement. A pixel represents one picture point on the Display. All measurements are calculated in picture points and are scaled appropriately by the operator or computer to obtain unnormalized results. The measurements which can be calculated are discussed below.

The 720 calculates the area of a detected feature as the number of detected or highlighted picture points that fall within the Live Frame. The actual area can be obtained by applying a calibration factor. Area can be obtained from the 1-D Auto Detector, Standard Analyzer and the Function Computer.

Horizontal Intercept is the total number of horizontal scans lines which intercept the trailing edge (right-hand edge) of a detected feature within the Live Frame. Vertical intercept applies the same logic in the vertical region. The horizontal and vertical intercepts can be measured simultaneously with the MS3 and Computer Controller, or sequentially by rotating the scanner ninety degrees between measurements. Chord sizing can be applied to select only chords greater than or less than a given size. Intercept can be used to derive measurements such as mean chord length, mean linear intercept, etc. Horizontal intercept can be computed in the MS3 and Function Computer. On the Function Computer it is called horizontal or vertical projection.

The perimeter function gives the total perimeter of all detected regions within the live frame. Any part of the perimeter that is in the guard region is excluded from the calculation. Perimeter, unlike most functions, is unaffected by chord sizing logic. It is calculated in the MS3 or Function Computer Module.

The four different methods to determine the number of features in a field are end-count, fork-or branch-count, topological-count and full-feature-count. Full-feature-count is the most useful method and will be the only method described. It counts the number of features whose A.C.P. (anti-coincidence point) lies within the live frame. By counting A.C.P.s rather than full features that are within the frame, a number of possible errors are eliminated, such as counting a feature that extends into the guard region

twice in two successive frames. Counting may be subject to a variety of tests such as sizing logic or any function on the Function Computer. By sequentially applying the proper tests, a size distribution chart can be accumulated. Counting can be obtained from the MS3 and Classifier Collector Module.

The feret measurement gives the diameter of an object in the direction of a given axis, e.g., vertical feret measures the height of an object. Horizontal and vertical feret are obtained from the Function Computer while feret values on a forty five degrees or one hundred thirty-five degrees axis can be calculated by the FIFI.

Pattern recognition is used when the desired detected feature cannot be isolated by grey-level criteria alone, but must be identified by its shape or dimensions. The easiest way to do this is by a man-machine interaction where a human operator selects the required feature and identifies it with the Light Pen. It is also possible to obtain simple pattern recognition by applying two logic tests, sizing logic and a function established by the Function Computer and Classifier Collector. If automation is desired, the 720 should have a computer controller where a program can be written using area, perimeter, various feret diameters and other functions to identify the desired particle. Pattern Recognition is selected on the MS3 module, but utilizes the functions of the MS3, Function Computer, and Classifier Collector. If the system is automated the FIFI and Control Interface are involved.

## 2. Types of Measurements Using the Quantimet 720

The Quantimet 720 is able, through its various functions, to obtain a number of useful measurements. Data can be obtained with one function, such as area, to find the total area of all particles in a frame. More complex data can be obtained by using a string of two functions, such as calculating

the total area of all particles in a frame with a chord size greater than ten pixels. With the computer controller present a program can be written with no limit on the number of functions in a string to compute data. Complex particle recognition can be used to differentiate detected features. For example, one could determine the total area, perimeter and location of all particles with horizontal feret greater than 15 pixels and vertical feret less than 25 pixels. It is also possible to gather information from a number of frames. One can obtain a measurement from one frame and move to the next frame to collect data.

To support the present research project the Quantimet will be used to obtain particle size distributions from a hologram. The Computer Controller will be utilized with a program that steps through a hologram, sums frames to eliminate noise (seen as snow on the Display), differentiates particles by grey levels and diameter, and sums the total area of particles in various ranges of diameter. Presently, the size distribution is being obtained with the enhanced basic Quantimet 720, utilizing the Light Pen and an operator.

### 3. Limitations of the Quantimet 720

The Quantimet 720 has a number of limitations which lead to inaccurate results. It cannot distinguish between particles and the background when the particles are at different grey levels in one frame. To distinguish the particles the frame size must be decreased or rearranged until only particles of the same grey level are within a frame. In addition, the 720 cannot provide accurate measurements when the field is unevenly illuminated. Once again, the field must be varied until it only contains a uniformly illuminated frame.

There are also errors introduced in the process of obtaining the image, converting it to a digital signal, and applying it to various logic tests in

separate modules. When obtaining the image, an error is introduced because the camera does not respond equally to the same grey level throughout the frame, i.e., an object with a grey level of X will be recognized at grey level Y in one part of the frame and grey level Z in another part of the frame. As the signal passes through the various modules, noise is added which degrades measurements. The 720 is also unable to determine the precise edge of a particle. It identifies the edge by noting areas where there is a sharp change in grey levels. The edge is determined by finding the greatest and least grey level and placing the edge exactly between the location of those levels. Of course, the edge may not be at that point and the greater the distance between the grey level extremes, the greater the possibility for error and amount of error. There are other limitations, but these are the major ones.

#### 4. Procedure for Obtaining Measurements

The purpose of the research being conducted is to obtain a distribution of the particles, by diameter or area, that exist in the combustion chamber of a small solid propellant rocket motor. The firing of the motor is recorded in a fifty nanosecond exposure of a hologram. One method for obtaining the needed data is to size the particles while stepping through the hologram reconstruction volume. In this initial investigation the equipment necessary for the Quantimet 720 to view the hologram reconstruction directly was not available. Therefore, another method had to be found which would determine how well the 720 could view a hologram and obtain the desired data. Since the Quantimet was capable of obtaining data from either a transparency or photograph, it was decided to record a plane of the reconstruction volume on film and to produce a photograph for use in the epidiascope.

The accuracy of this method is dependent on the quality of the photograph obtained. To insure that this objective was met, care was taken in selecting the proper film, using a quality camera and lens system, selecting a good image to be photographed and monitoring the developing process to insure that it was done correctly. A high-quality film, Kodak TRI-X ASA 400, was selected. The camera was a Canon F-1 and the hologram was viewed through a Gaertner microscope. The microscope objective was a 1X lens and the eyepiece was a 5X lens, the combination providing 5X magnification.

Figure 40 shows the equipment and setup used to photograph a frame of the reconstructed hologram. As shown in Figure 41, the equipment consisted of a camera, a microscope, a spinning mylar disk located at the focal point of the microscope (with the reconstructed real image projected onto it), a holocamera box and the krypton-ion laser. The shutter speed was set at five seconds or greater when the photograph was taken.

Choosing a proper frame from the photograph when placed on the Quantimet was difficult. Earlier work with the Quantimet had shown that the best results were obtained when a frame was uniformly illuminated and the particles of interest were at similar grey levels. The grey level of a particle was strongly dependent on illumination, therefore particles with similar grey levels were obtained by selecting a frame with even illumination.

A photograph must also be taken of the 0-80 screw (or other objects for sizing particles) in the rear of the hologram to provide a reference measurement. When the hologram was constructed the screw was placed outside the burning motor, but within the depth of field of the hologram. This was done so that a calibration constant could be derived, knowing that the

distance from ridge to ridge on the screw was 317 microns. The screw must be photographed at every magnification that data frames are photographed to obtain the correct calibration constant for all magnifications. One must also insure that during the developing process that the data image and its respective calibration image are enlarged equally for the prints. A good print size is approximately 2 inches by 3 inches since the Quantimet can view that area with six frames.

The photographs to be used for data and their respective calibration photo were first selected. Before data can be obtained from the photo it is best to first obtain the calibration factor. After setting up the Quantimet for the desired measurements, one places the calibration photograph on the epidiascope, then the scale is overlaid (controlled by the Variable Frame and Scale Module) on the image of the threads to determine the number of pixels between the threads. The calibration factor is calculated as:

$$C.F. = \frac{\text{physical distance between threads}}{\text{number of pixels between threads}}$$

With this constant the values obtained with the Quantimet can be converted to physical values.

A photograph to be analyzed is then selected and placed on a piece of graph paper using a horizontal and a vertical line as the X and Y axis. The (0,0) point should be in the lower left-hand corner and the axis should be numbered. The photo is placed on the epidiascope so that the complete photograph can be viewed by the scanner by moving the stage. The X and Y axes must be visible for they will serve as points of reference as one is moving the stage through a frame. It is also helpful to find the relationship between the units on the graph paper and those on the X-Y stages. The stage is moved so that the (0,0) point is at the lower left-hand corner and the

axes are on the edge of the screen. The necessary range of movement of the stage in the horizontal and vertical direction is determined, as are the number of frames that will have to be measured. For example, if the picture is a two-inch square and a one-inch square is displayed on the screen, it will take a minimum of four frames to gather all data.

Returning to the origin, the image is studied on the display. To obtain data, the Quantimet needs a uniform illuminated field. If the image on the display has uneven illumination, the frame must be varied with the Variable Frame and Scale Module, until an image of even illumination is obtained. To find the area or diameter of a particle, the desired function on the Function Computer is set and the Light Pen is pointed at the particle, providing the required measurement. One can also use sizer logic and let the 720 find the total area of particles in a frame with the largest horizontal chord greater than a set value. Particles should be grouped by area or perimeter since diameter and chord sizing are dependent on the particle orientation. One continues to move through the photograph by moving the stage and varying the frame size and detection level when necessary. If a particle is partially in a frame, the frame size is varied on the next move so that the complete particle is contained within the new frame.

By varying the grey level for detection one also varies the values obtained. To overcome this problem, when moving from frame to frame, the frame size can be altered so that a particle which was recorded in the last sequence appears in the new frame. The detection level is adjusted so that the particle has the same area as it did in the prior frame. If this is not possible, the proper detection level should be set on objects which are in focus. In this manner accurate values can be obtained when moving from frame to frame and varying the detection level.

## C. RESULTS AND DISCUSSION

### 1. Demonstration of Data Reduction

Figure 42 is a photograph that was analyzed with the Quantimet 720 and Figure 43 shows the detected regions. The image is a frame from a reconstructed hologram of a WGS-ZrC propellant burn made at 36 atm. The photo was analyzed as described above to obtain the area size distribution listed in Table IV. The Light Pen was used to identify particles of interest and size logic was used to eliminate noise. The calibration constant was found from the photo of the screw to be 165 pixels/317 microns. With this information the conversion between pixels and microns was made to construct Table IV.

Table IV Distribution of Particles from a Plane of a Hologram of a WGS-ZrC Burn

# of Particles	Area, ( $\mu\text{m}^2$ )
11	0 - 3999
6	4000 - 7999
5	8000 - 11999
2	12000 - 15999
2	16000 - 19999
1	20000 - 39999
1	> 40000

Although this frame was analyzed manually with the light pen, one could also use the Function Computer and Classifier Collector to automate the process. This would be done by counting the number of particles that fall within area limits until all particles are classified and counted. In this example the number of particles with an area between 100 and 200 pixels are counted, then the limits are increased to count the number of particles with

an area between 200 and 300 pixels. The limits are incremented until the number of particles that fall within the bands have all been counted. This method was not used since it was more time consuming to go through every frame and manually switch the area limits for each sizing. Under computer control this method would be much quicker since the computer could step through the area blocks, automatically count the particles in the respective limits and move to the next frame. It would also avoid counting particles more than once since the particles are only counted when the A.C.P. lies within the Live Frame.

## 2. Sources of Error

There are four primary sources of error when obtaining data from a visual image of a reconstructed hologram of solid propellant combustion using the Quantimet 720. The errors are due to speckle, uneven illumination, variances in the grey levels of particles and determining when particles are in focus.

Speckle can introduce a large amount of error to the measurements. Speckle has two effects on the reconstructed image. It produces black spots in the background which cannot be readily distinguished from real particles, except perhaps, by size and/or color gradients. The second observed effect of the speckle is that it gives the actual particle a "swiss cheese" appearance, which alters any calculated measurements on the particle, particularly area or perimeter. The Quantimet usually ignores the holes within the particle when measuring area, but significant error is introduced when the perimeter is altered.

The first effect limits the minimum size of particles that can be measured, i.e., the particles must be larger than the speckle. Speckle is the granular interference pattern superimposed on a coherent image. In

microscopy, speckle is of particular importance since the size of the speckle grains is frequently comparable to the size of the particles being imaged and measured. In the present apparatus, there appears to be two contributors to the formation of the speckle. The first occurs in the recording of the hologram. Objects illuminated with diffuse coherent light are subject to speckle in the interference of the illumination wave and the reference wave. Referring to Figure 44, the predicted speckle is given by (Reference 18)

$$d_{\text{speckle}} = \frac{\lambda}{\beta \cos \theta} \quad (4)$$

where  $\lambda$  is the laser wavelength,  $\beta$  is the angle subtended by the illuminating beam as seen from the object and  $\theta$  is the angle measured at the object between the axis to the center of the illuminated diffuser and the center of the image plane (the hologram). For the geometry of the present experiment,  $\lambda=676$  nm,  $\beta$  is approximately 62.4 mr, and  $\theta$  is 180 degrees, giving a speckle diameter at the hologram plane of 10.8  $\mu\text{m}$ . This speckle will be recorded by the hologram and will be present in the reconstructed image. The primary means of reducing the speckle size is to increase the illumination aperture of the diffuser or to decrease the distance from the diffuser to the object.

The second contributor to the speckle in the final image is that due to the imaging lenses. In the present system there are two imaging operations in the reconstruction process. The first is the formation of the real image on the mylar disk through the assisting lens set. The second is the imaging of the image on the mylar disk onto the TV tube face through the microscope lens. The minimum speckle diameter that will be imaged by an imaging lens such as shown in Figure 45 is given by (References 19 and 20):

$$d_{\text{speckle}} = \frac{1.22\lambda M}{2 \tan[\arcsin(NA)]} \approx \frac{1.22\lambda M}{2 \tan[NA]} \quad (5)$$

where  $M$  is the magnification of the imaging system (and is given by the ratio of the  $I/O$ ) and  $NA$  is the numerical aperture of the lens. The numerical aperture is given by approximately  $1/(2f_{no})$  or  $\arctan [d_{\text{lens}}/2(O)]$  where  $f_{no}$  is the  $f$ -number of the lens,  $I$  is the distance from the lens to the image plane,  $O$  is the distance from the lens to the object and  $d_{\text{lens}}$  is the diameter of the lens. Alternate forms of the equation are

$$d_{\text{speckle}} = \frac{1.22\lambda I}{d_{\text{lens}}} \quad (6)$$

or

$$d_{\text{speckle}} = 1.22\lambda(1+M)f_{no} \quad (7)$$

The first imaging operation is the formation of the real image from the hologram through the assisting lens set. Although the lens set is involved in the imaging, the hologram itself is the primary imaging element. A model has to be developed that would model the image formation with an equivalent lens and would incorporate the effects of the assisting lens set. This work is currently in progress.

The second imaging operation is the imaging performed by the microscope objective onto the image tube of the camera. (The eyepiece is removed for this operation.) The minimum speckle size is predicted by Equation 7, and is plotted in Figure 46. Reduction of the minimum speckle to values below 3 or 4  $\mu\text{m}$  requires  $f$ -numbers below 0.4 for magnifications of 10x. For magnifications of 1x,  $f$ -numbers below 4 are adequate. Typical  $f$ -numbers of microscope objectives are in the range of 1.5 to 10 for this range of magnification,

indicating that magnifications of 2x or so, are consistent with reducing the speckle size to values similar to the smallest particles.

Generally, the conclusion is that, to reduce the size of the speckle, large aperture optics are desirable since it is experimentally confirmed that speckle diameter is reduced as the numerical aperture of the imaging elements is increased (References 21 and 22).

If the speckle cannot be made negligible compared to the object image features, other techniques might be available to average out the speckle. These techniques are based on the fact that the speckle pattern will shift if one or more of many variables is changed while the object image will remain fixed in position. By averaging  $N$  images with differing speckle patterns, an improvement of the object brightness to speckle brightness on the order of  $N^{1/2}$  will result. With enough improvement the speckle pattern can theoretically be made insignificant compared to the object pattern, although the value of  $N$  may be impractically high. Variables that can be changed to cause a significant shift in the speckle pattern while causing only minor changes in the object pattern are: changing the imaging aperture, changing the object position by small amounts, illuminating different regions of the diffuser, or moving the longitudinal position of the image screen (or equivalently, the longitudinal position of the imaging lens). Each of these techniques usually changes the object image to some extent and frequently major efforts are required to minimize this change.

Uneven illumination can also cause significant errors if not dealt with properly. As discussed earlier the Quantimet differentiates objects by determining differences in grey levels. If two in-focus particles of equal size are illuminated at different values of intensity, they will be detected at different grey levels by the 720, and different measured values of size can

be obtained. The reason for this is that the eye tends to smooth out small differences in grey levels and views the objects as being at one grey level. The Quantimet does not smooth out the difference in grey levels but accurately sees the particles as a number of concentric shapes, each at a different grey level, with the darkest value in the center and decreasing darkness toward the edges. If particles have received different amounts of illumination, the outside perimeters will be at different grey levels. With the Quantimet set to measure all pixels darker than a set grey level, one can easily see how in a frame with less illumination the area of the particle will be calculated at a greater value than the frame with more illumination. Figure 47 demonstrates how this occurs. The two equal-sized particles under different illumination are shown. The number in each band is the grey level of that band (level 0 is total darkness). If the Quantimet is set to calculate the area of objects darker than grey level 20, the radius of the detected circle would be  $R_1$  in the low illumination case. In the high illumination case the detected region would be bounded by the smaller radius  $R_2$ .

Uneven illumination has two sources; the illumination of the hologram and the uneven illumination of the photograph by the lights in the epidiascope. In the hologram the differences in illumination level are due to shadowing from particles and attenuation due to smoke and various gradient effects. On the epidiascope the light source which illuminates the photograph consists of four bulbs. The intensity of the bulbs can be varied, but it is almost impossible to adjust them so that all points on the photograph are illuminated equally. The Quantimet attempts to correct this uneven illumination due to the epidiascope by using a shading corrector circuit.

Uneven illumination causes an error in measurement since the detection level is improperly set. In the earlier example the correct values can be obtained if the frame is broken up into two frames. The frame with low illumination should be evaluated with a detection level of less than or equal to grey level 20 and the highly illuminated frame should be evaluated at less than or equal to grey level 25. To obtain the proper measurements in a frame with a number of particles, the correct level for detection should be set on a particle in focus. Using this method an algorithm could be written to count and measure the number of particles in a hologram with uneven illumination. The procedure would be to select a field with equal illumination by cutting down the test area until such a field is obtained. Then the level of detection is set on a particle that is in focus and the desired measurements are taken.

Not being able to accurately determine when a particle is in focus can lead to a number of errors. The "in-focus" criterion is used to determine the boundary of a particle for measurements and the correct detection level setting. Clearly an inaccurate determination can lead to significant errors in measurements since the actual boundary location is unknown.

The primary reason for focusing errors is that a hologram is a three-dimensional view of an object, but the Quantimet must analyze data in two dimensions. The third dimension of the view is obtained by stepping through the real image and successively analyzing a 2-D picture at each step. When the observer is moving through the hologram, particles will appear in and out of focus. Only particles which are in focus will be analyzed since the edges are well defined and accurate measurements can be obtained. Objects which are out of focus will be analyzed in later frames when they will be in focus. By using this logic one also avoids counting the same particle in successive

frames since it should only be in focus in one frame. The difficulty arises in determining when a particle is exactly in focus. A particle that is in focus is characterized by being darker and having a sharp change in grey levels at the edges. A particle near the focal plane, i.e., not in focus, will have a gradual change of grey levels.

There are two methods for determining when a particle is in focus and should be counted. The first method is to leave the decision to a human operator. The second method requires an algorithm to be developed which determines when a particle is in focus, thus automating the decision. A possible test would be to state that all images which change 10 grey levels in 3 pixels or less be considered in focus.

The Quantimet 720 introduces some errors in measurements, but it is felt that these are insignificant compared to the previously listed ones. Nevertheless, one should be aware of these errors. The two that appear most often are described below.

The Quantimet does not detect features equally across the total field of view. For example, a particle could be detected at level 20 in the lower left-hand corner of the display and be detected at 25 in the upper right hand side. The automatic shading circuit attempts to correct this problem but it still causes errors in some locations.

The Quantimet also introduces noise in the system which is seen as randomly located detected points. These points are included in all calculations, thereby introducing errors in the measurements. The counting function is particularly sensitive to this type of error. When counting the number of objects in a frame, the 720 may show 3 times the amount of particles present since it counts the noise as particles too. This error can be largely eliminated by sizer logic to eliminate the very small noise points.

## D. CONCLUSIONS AND CURRENT EFFORTS

### 1. Installation

The Quantimet 720 has been installed and is now capable of performing all basic operations. The basic operations consist of measuring area, perimeter, number of features in a field, and horizontal and vertical feret. Some automation is possible using the pattern recognition mode, where two logic tests can be performed to obtain data on particles which pass the set logic test. To assist in future installation a wire list has been developed showing the required interconnection of the modules.

The Computer Controller has been purchased. The controller is a Digital Equipment Corporation (DEC) PDP 11/04 computer with 64K MOS ROM, serial and parallel ports, dual disk drives and a DECWRITER. The computer and its components have been tested and are operational.

The motorized XYZ stage has also been purchased. A base has been manufactured that allows the stage to be mounted on the optical bench. The holocamera is located on top of the stage. Movement through the hologram is accomplished by the stage changing the holocamera location.

### 2. Testing and Operation

The Quantimet 720 has demonstrated that it can be readily used to obtain particle size distributions from a photographed frame of a hologram. The method used to extract the data is described and an operator's manual has been written due to the inadequate documentation provided. A description of the errors present and possible solutions has also been provided.

### 3. Planned Efforts

Complete installation of the Quantimet 720 in the advanced mode with the Computer Controller could not be attained in the initial effort.

The system will be upgraded to a semiautomatic Quantimet 720 by use of the Computer Controller and motorized XYZ stage. The block diagram in Figure 48 shows all the components necessary to accomplish this. The following steps will be taken:

(a) The Computer Controller will be interfaced with the Quantimet 720 through an interface cable connecting the FIFO and DMA board in the PDP 11/04. Through the use of Q software, which must be installed with an RX-11 version 3 operating system, DMA transfers will be allowed and Q software functions will be possible. Q software provides control of the Quantimet functions through the computer rather than individual modules.

(b) The XYZ stage installation will be completed. The holocamera will be mounted on the stage which can provide submicron positioning. Instructions can be given by the standard controller or from the computer through a RS-232 port.

(c) The scanner will be interfaced with the microscope so that direct viewing of holograms is possible. The components are now present but some testing must be done to determine if additional lenses are needed and which lenses provide the best interface.

(d) Efforts at understanding and minimizing the speckle in the image will continue. The recording geometry and choice of optical components will be refined in an effort to reduce the present speckle content.

## REFERENCES

1. Karagounis, S. G., Gillespie II, T. R., Hickey, P. J., Diloreto, V. D., Dubrov, E., Netzer, D. W., An Investigation of Experimental Techniques for Obtaining Particulate Behavior in Metallized Solid Propellant Combustion, AFRPL-TR-82-051, Air Force Rocket Propulsion Laboratory, July 1982.
2. Boggs, T. L., Crump, J. E., Kraeutle, K. J., Zurn, D. E., "Cinephotomicrography and Scanning Electron Microscopy as Used to Study Solid Propellant Combustion," Progress in Astronautics and Aeronautics, Volume 63, Experimental Diagnostics in Combustion of Solids, pp. 20-48.
3. Dobbins, R. A., Jizmagian, G. S., "Optical Scattering Cross Sections for Polydispersions of Dielectric Spheres," Journal of the Optical Society of America, Volume 56, Number 10, 1966.
4. Dobbins, R. A., Jizmagian, G. S., "Particle Size Measurements Based on Use of Mean Scattering Cross Sections," Journal of the Optical Society of America, Volume 56, Number 10, 1966.
5. Gumprecht, R. O., Sliepeevich, C. M., "Scattering of Light by Large Spherical Particles," Journal of Physics and Chemistry, Number 57, 1953.
6. Chin, J. H., Sliepeevich, C. M., Tribus, M., "Particle Size Distribution in Polydispersed Systems by Means of Measurements of Angular Variation of Intensity of Forward-Scattered Light at Very Small Angles," Journal of Physics and Chemistry, Number 59, 1955.
7. Dobbins, R. A., Crocco, L., Glassman, I., "Measurement of Mean Particle Sizes of Sprays from Diffractively Scattered Light," AIAA Journal, Volume 2, Number 3, 1964.
8. Muggels, R. A., Evans, H. D., "Droplet Size Distribution in Sprays," Industrial Engineering and Chemistry, 43, 1951.
9. Roberts, J. H., Webb, M. J., "Measurements of Droplet Size for Wide Range Particle Distributions," AIAA Journal, Volume 2, Number 3, 1964.
10. Hodkinson, J. R., "Particle Sizing by Means of the Forward Scattering Lobe," Applied Optics, Volume 5, Number 5, 1966.
11. Nejad, A. S., Schetz, J. A., Jakubowski, A. K., "Mean Droplet Diameter Resulting from Atomization of a Transverse Liquid Jet in a Supersonic Air Stream," AFOSR-TR-79-0004, November 1978.
12. Powell, E. A., Cassanova, R. A., Bankston, C. P., Zionn, B.I., "Combustion Generated Smoke Diagnostics by Means of Optical Measurement Techniques," AIAA 14th Aerospace Sciences Meeting, January 1976, AIAA Paper Number 76-67.

13. Buschele, D. R., "Particle Sizing by Measurement of Forward-Scattered Light at Two Angles," NASA-TP2156, 1983.
14. Briones, R. A., Wuerker, R. F., "Instruction Manual for the Improved Ruby Laser Holographic Illuminator," AFRPL-TM-78-11, Air Force Rocket Propulsion Laboratory, July 1978.
15. Wuerker, R. F., Briones, R. A., Operation Manual for the Lens-Assisted Multipurpose Holocamera with Reflected Light Option, AFRPL-TM-78-12, Air Force Rocket Propulsion Laboratory, July 1978.
16. Klein, N., Dweilde, M. A., "Pulsed Holography for Combustion Diagnostics," 17th JANNAF Combustion Meeting, September 1980.
17. Cambridge Instruments, "Instruction Manual Quantimet 720," 40 Pitt Dr., Monsey, New York, 1976.
18. Francon, M., Laser Speckle and Applications in Optics, pp. 33-34, Academic Press, 1979.
19. Erf, Robert K., "Applications of Laser Speckle to Measurements," Laser Applications, Volume 4, p. 7, Goodman and M. Ross, Academic Press, 1980.
20. Melles Griot, Optics Guide 2, p. 10, 1770 Kettering Street, Irvine, California, 1976.
21. Briones, R. A., Heflinger, L. O., Wuerker, R. F., "Holographic Microscopy," Applied Optics, Volume 17, Number 6, pp. 944-950, 15 March 1978.
22. Briones, R. A., Wuerker, R. F., "Experimental Diagnostics in Combustion of Solids," Astronautics and Aeronautics, Volume 63.

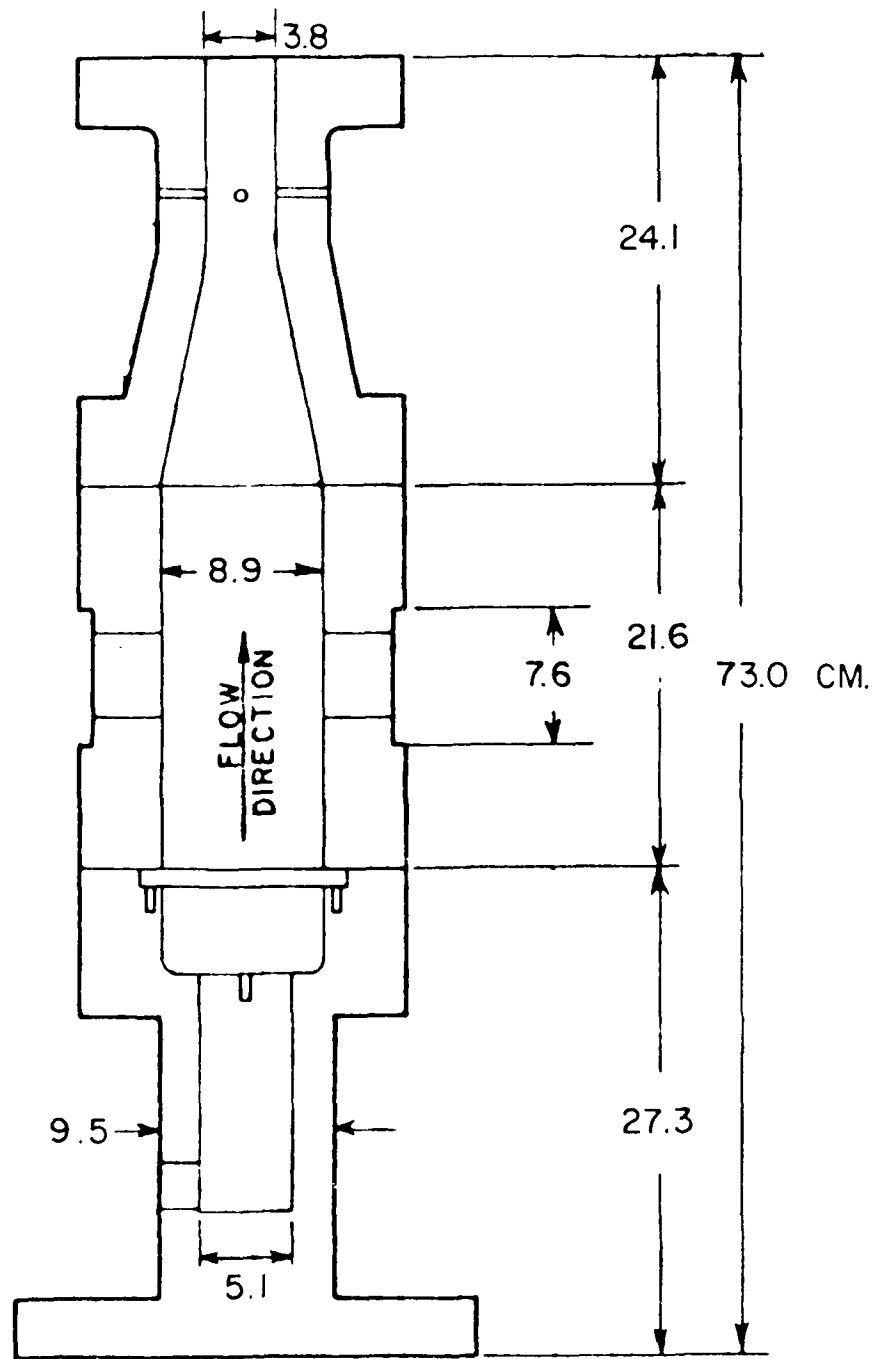


Figure 1. Schematic of Larger Combustion Bomb Showing Principal Dimensions.

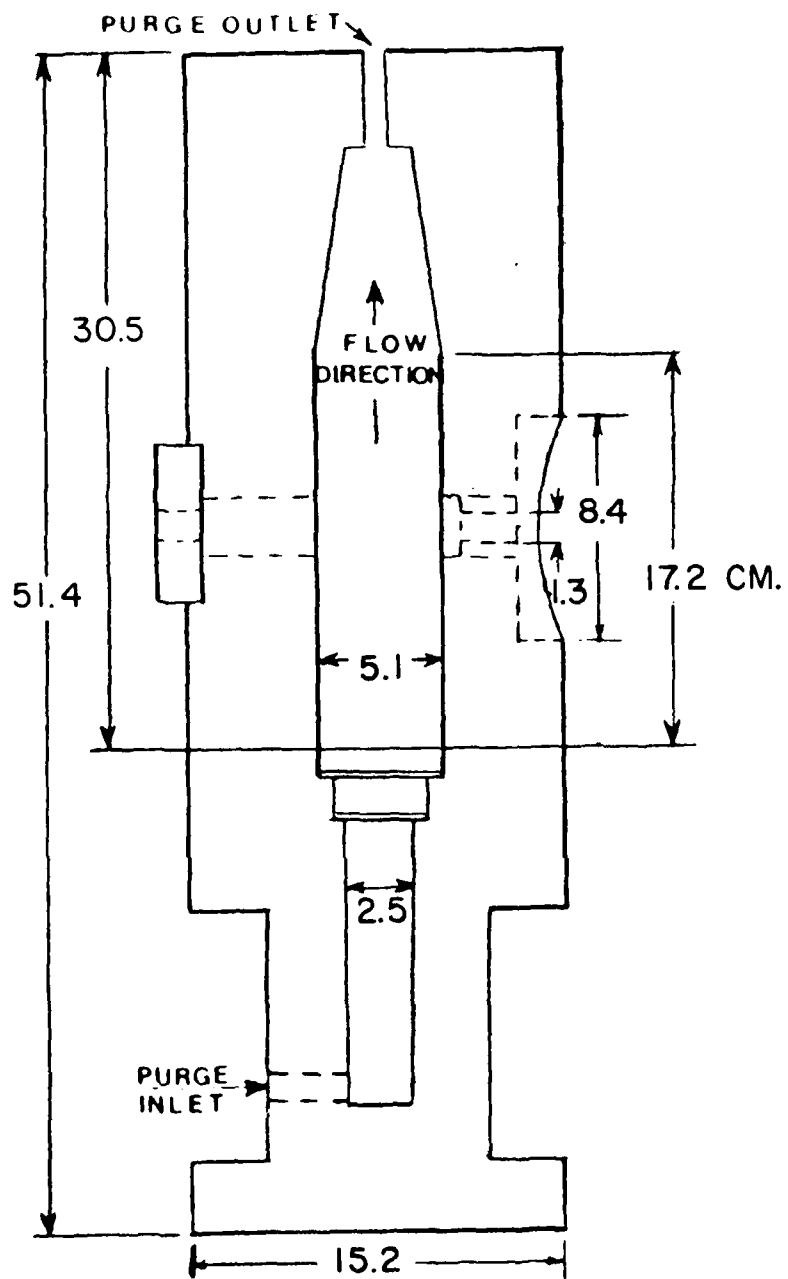


Figure 2. Schematic of High Pressure Combustion Bomb Showing Principal Dimensions.

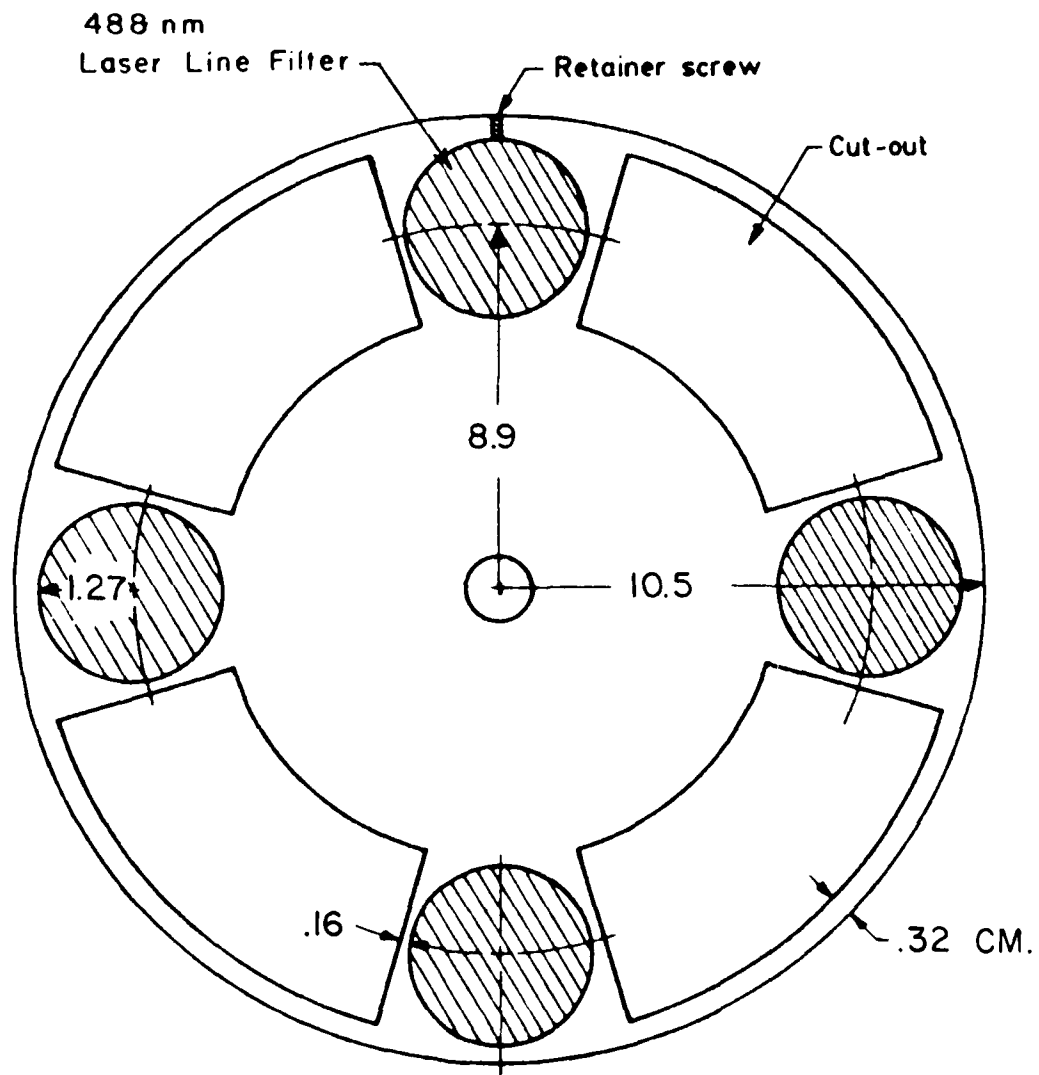


Figure 3. Schematic of Narrow Pass Filter Disk.

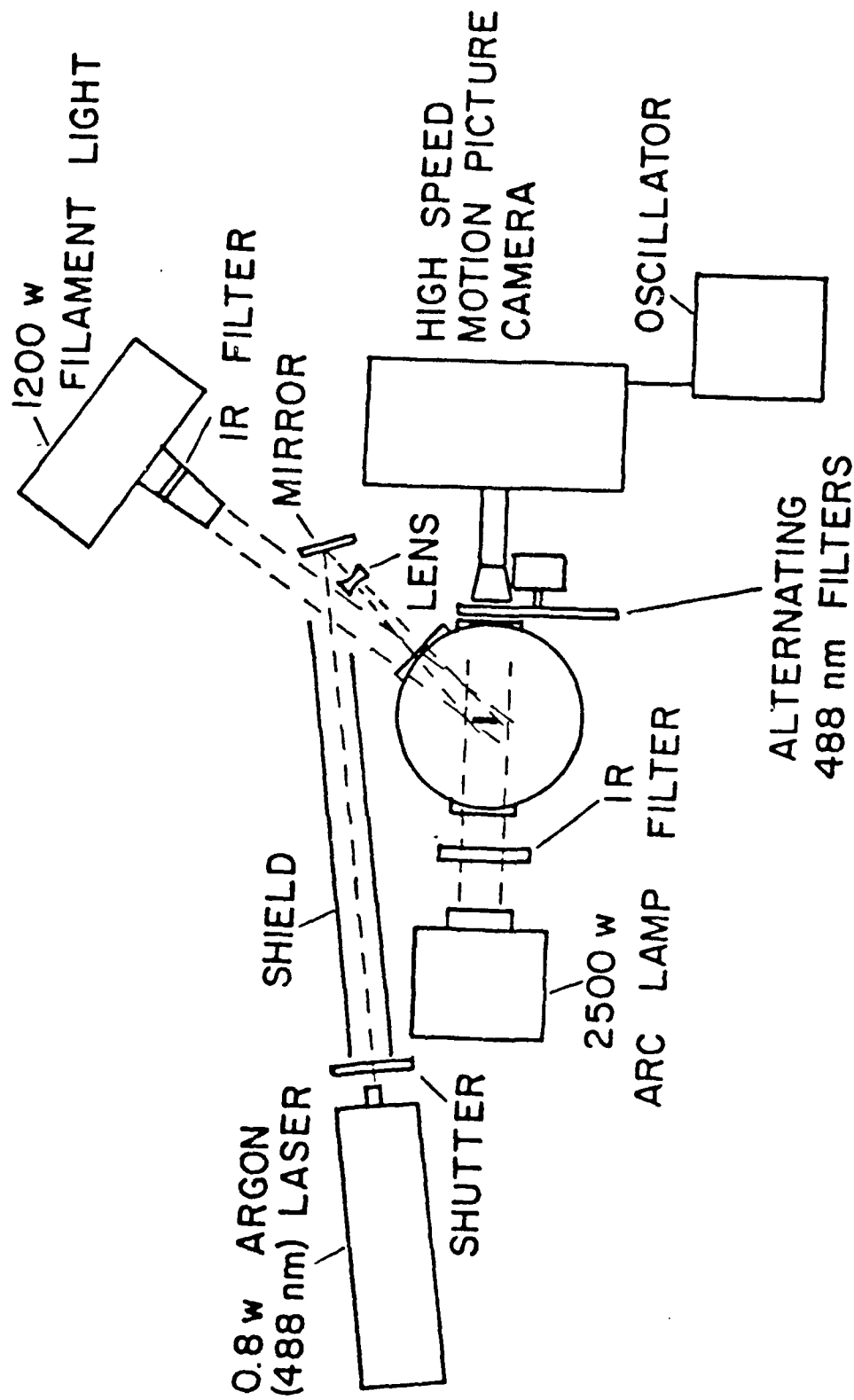


Figure 4. Schematic of Combustion Bomb Apparatus.

Figure 5. Photographs of Propellant WGS-6A Strands Burned at 34 atm. Pressure.

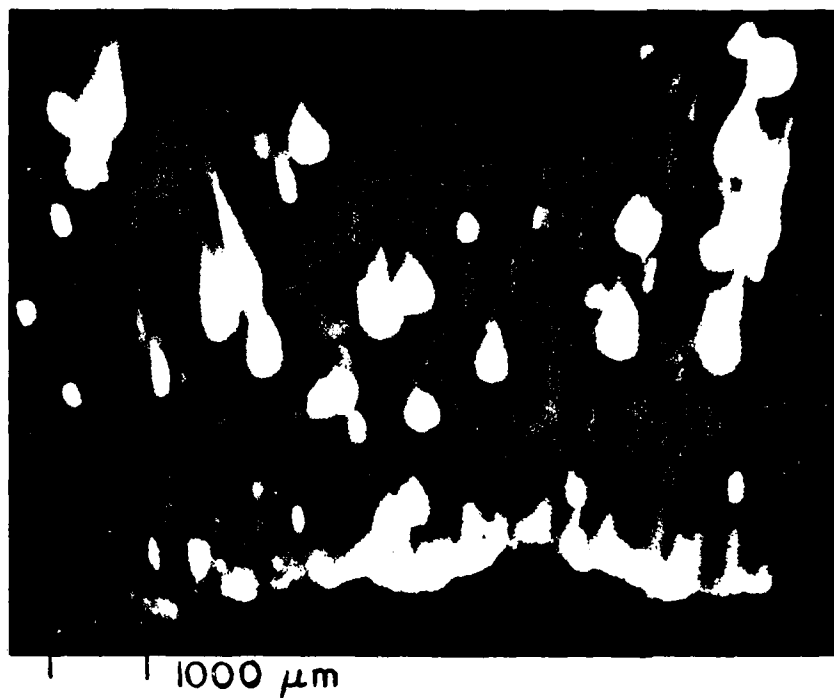


Figure 5a. high speed motion picture with minimum illumination.

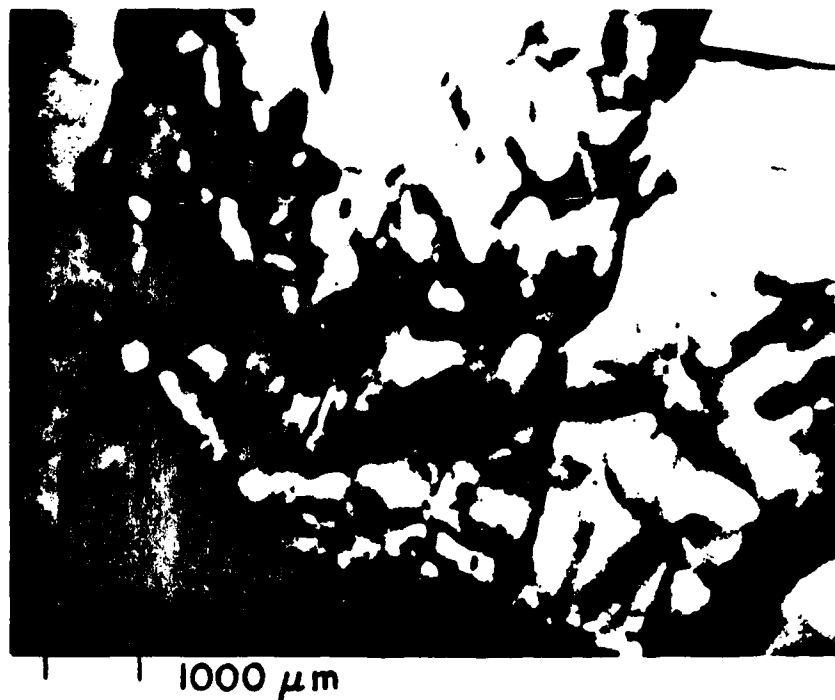


Figure 5b. high speed motion picture with 2500 watt rear illumination.



1000  $\mu\text{m}$

Figure 5c. reconstructed hologram.

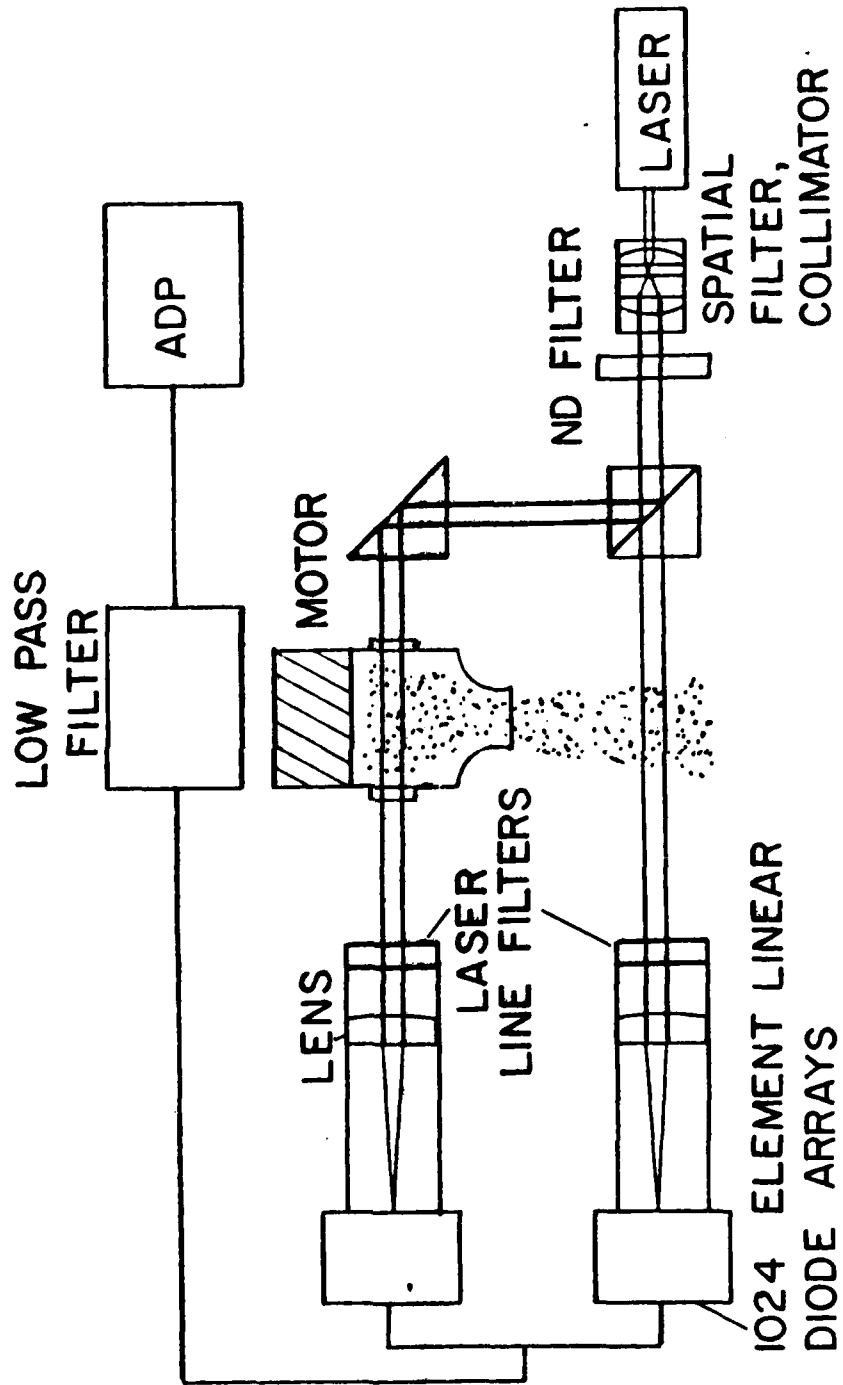


Figure 6. Schematic Diagram of Diffractively Scattered Light Apparatus.

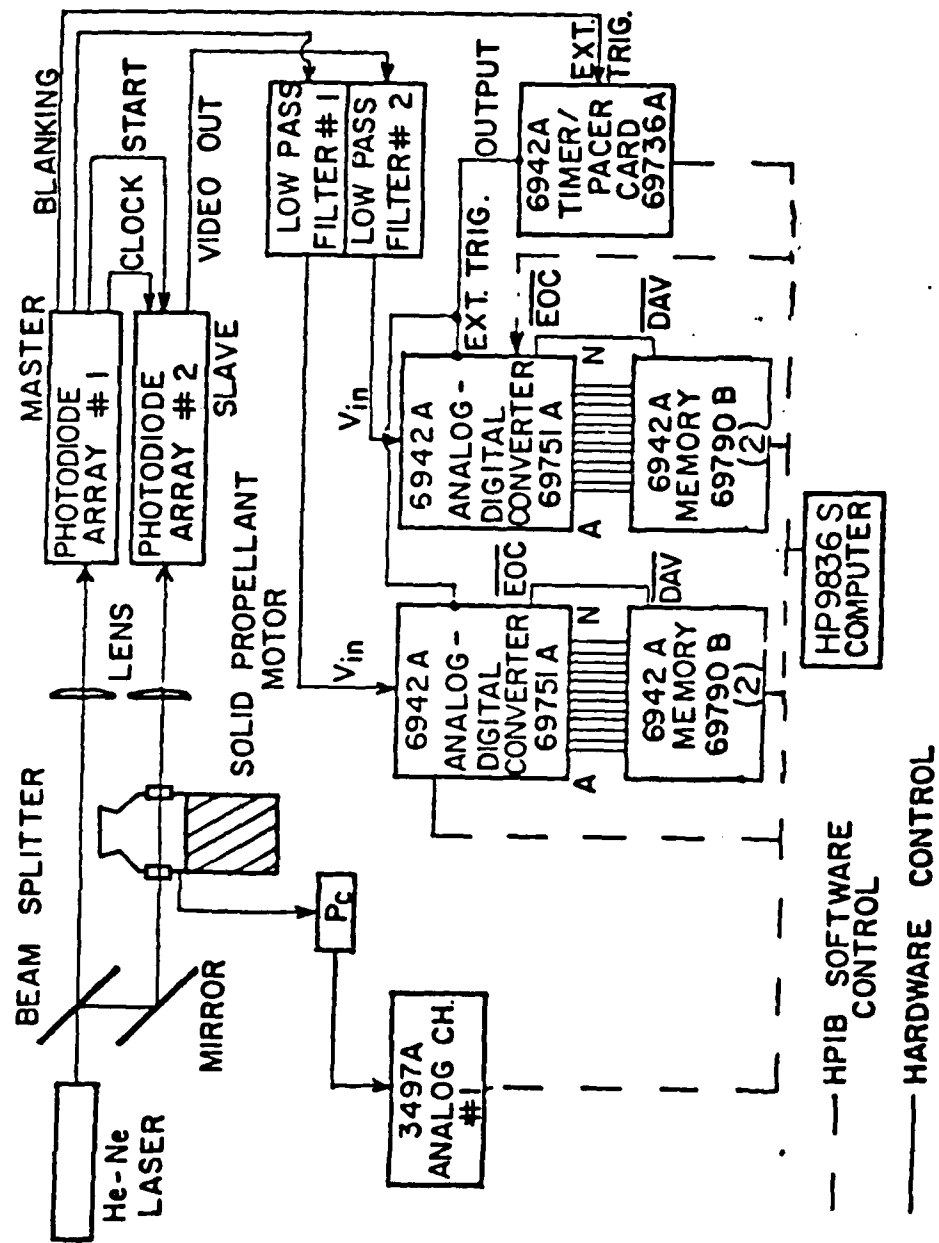
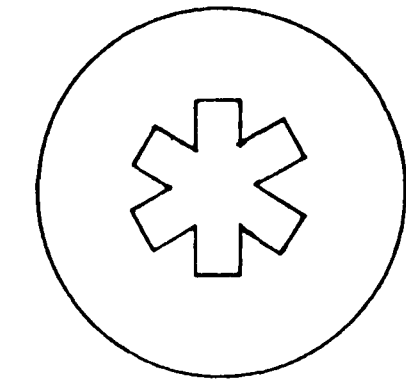


Figure 7. Schematic of Data Acquisition System for Light Scattering Measurements.



GRAIN DESIGN

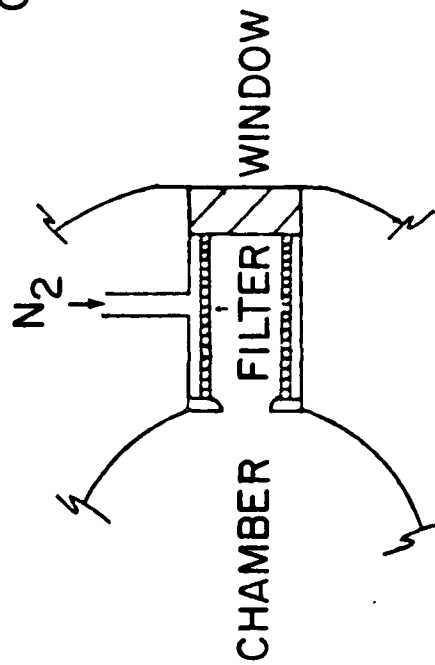
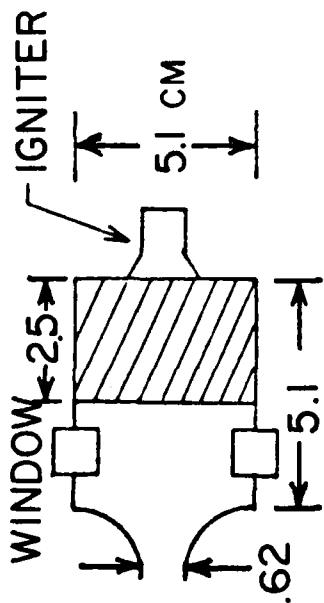


Figure 8. Small Motor Construction.

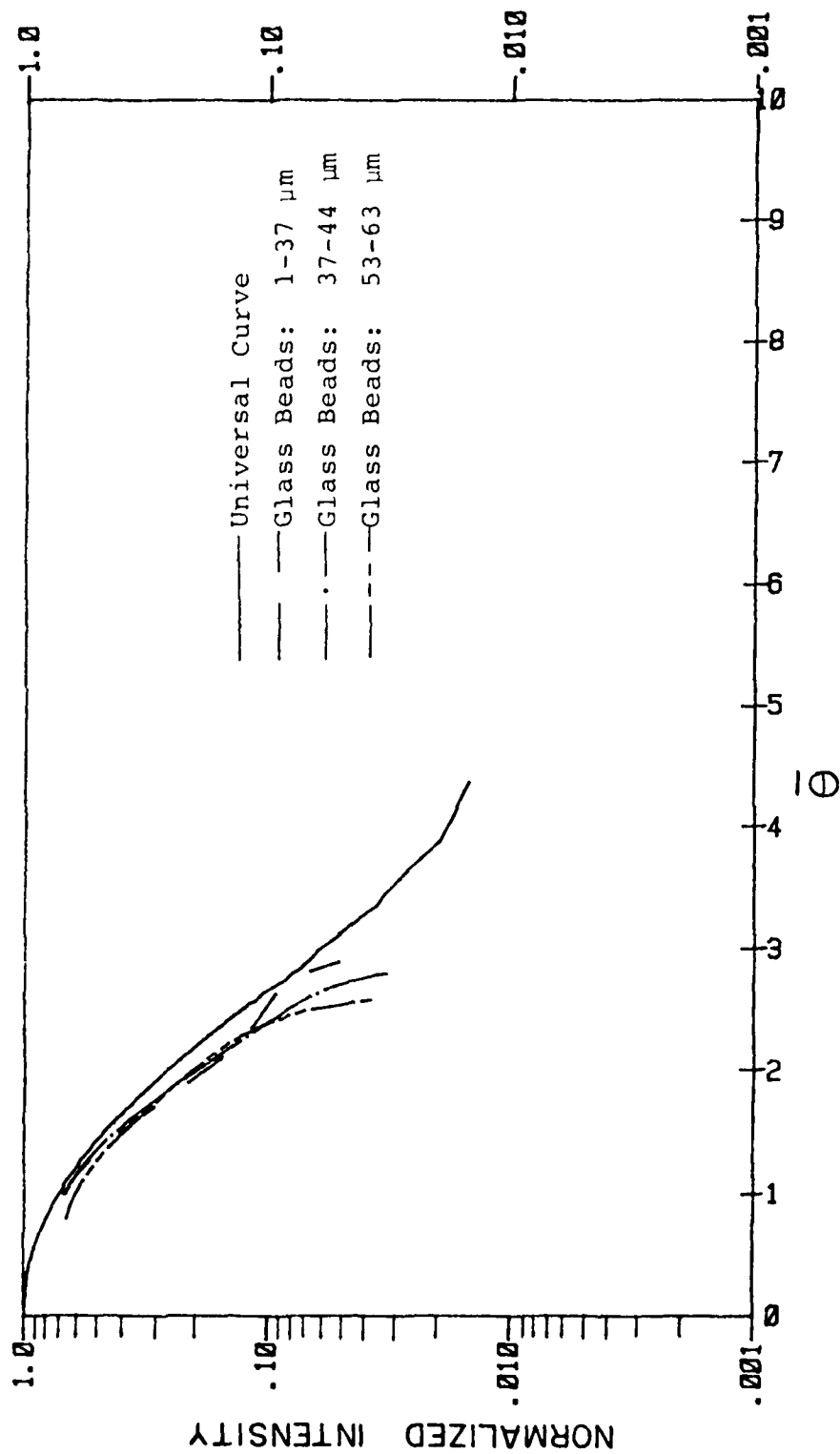


Figure 9. Normalized Intensity Profiles, Spherical Glass Beads.

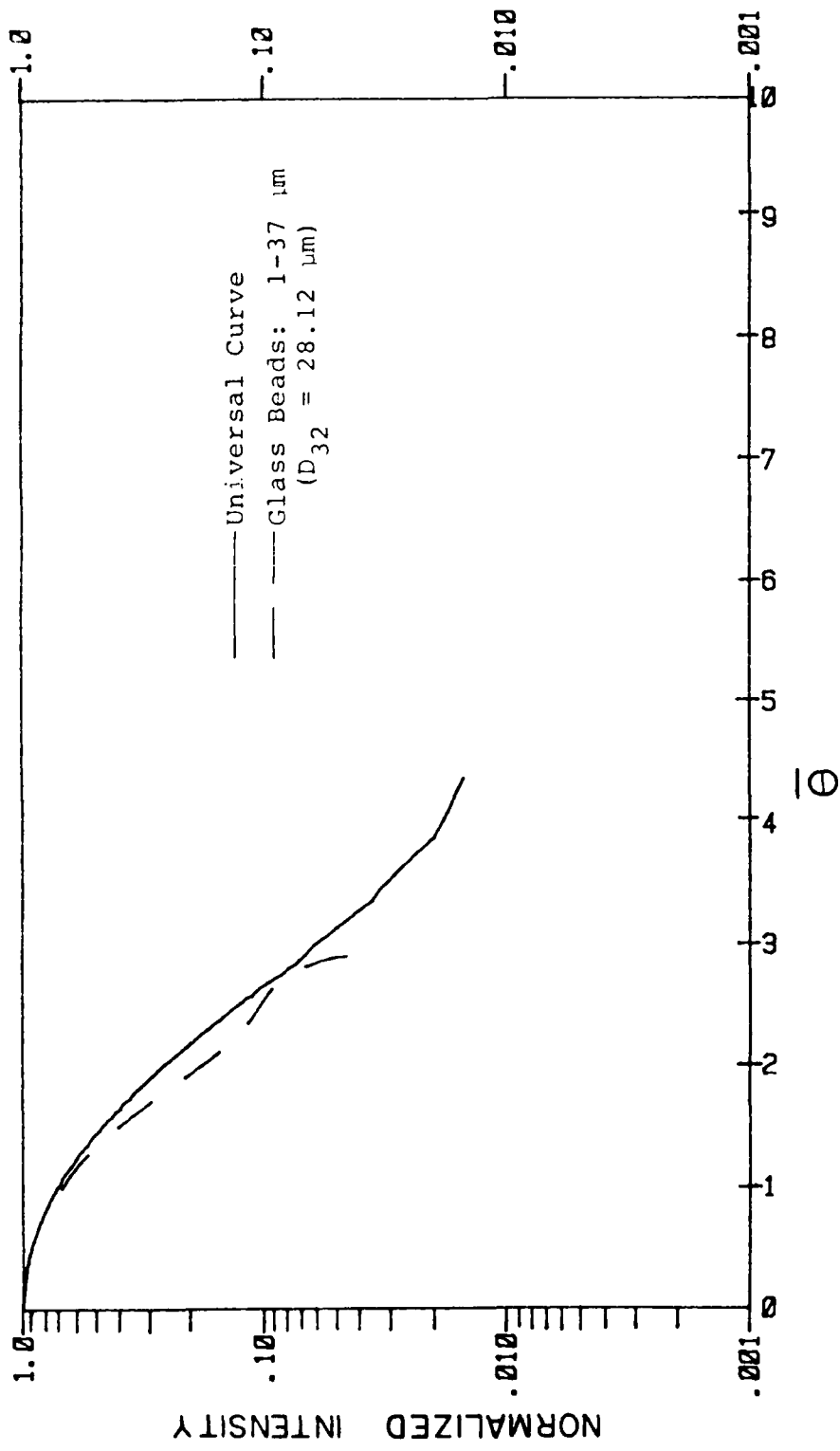


Figure 10. Normalized Intensity Profiles, 1-37  $\mu\text{m}$  Glass Beads.

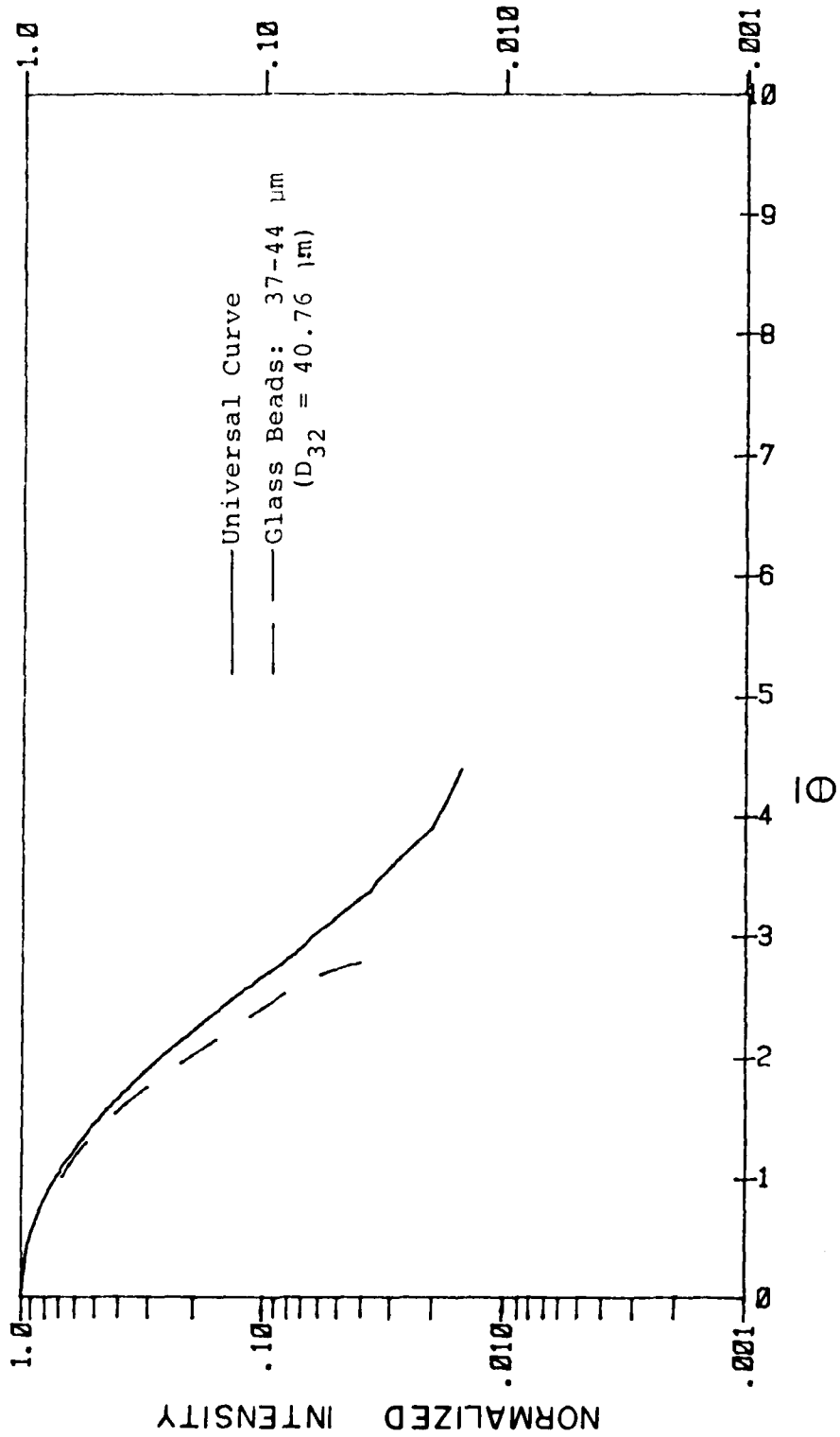


Figure 11. Normalized Intensity Profiles, 37-44  $\mu\text{m}$  Glass Beads.

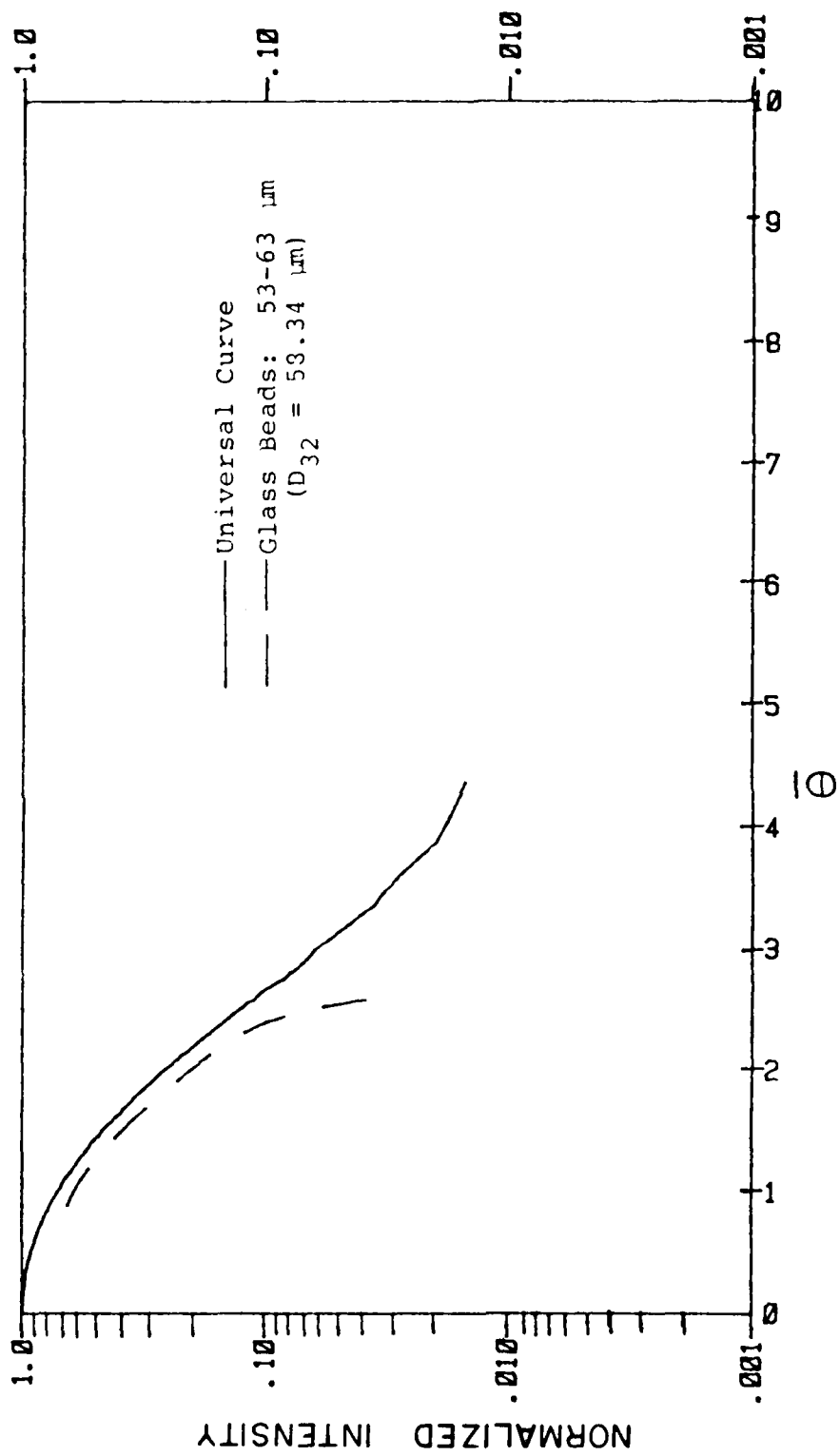


Figure 12. Normalized Intensity Profiles, 53-63  $\mu\text{m}$  Glass Beads.

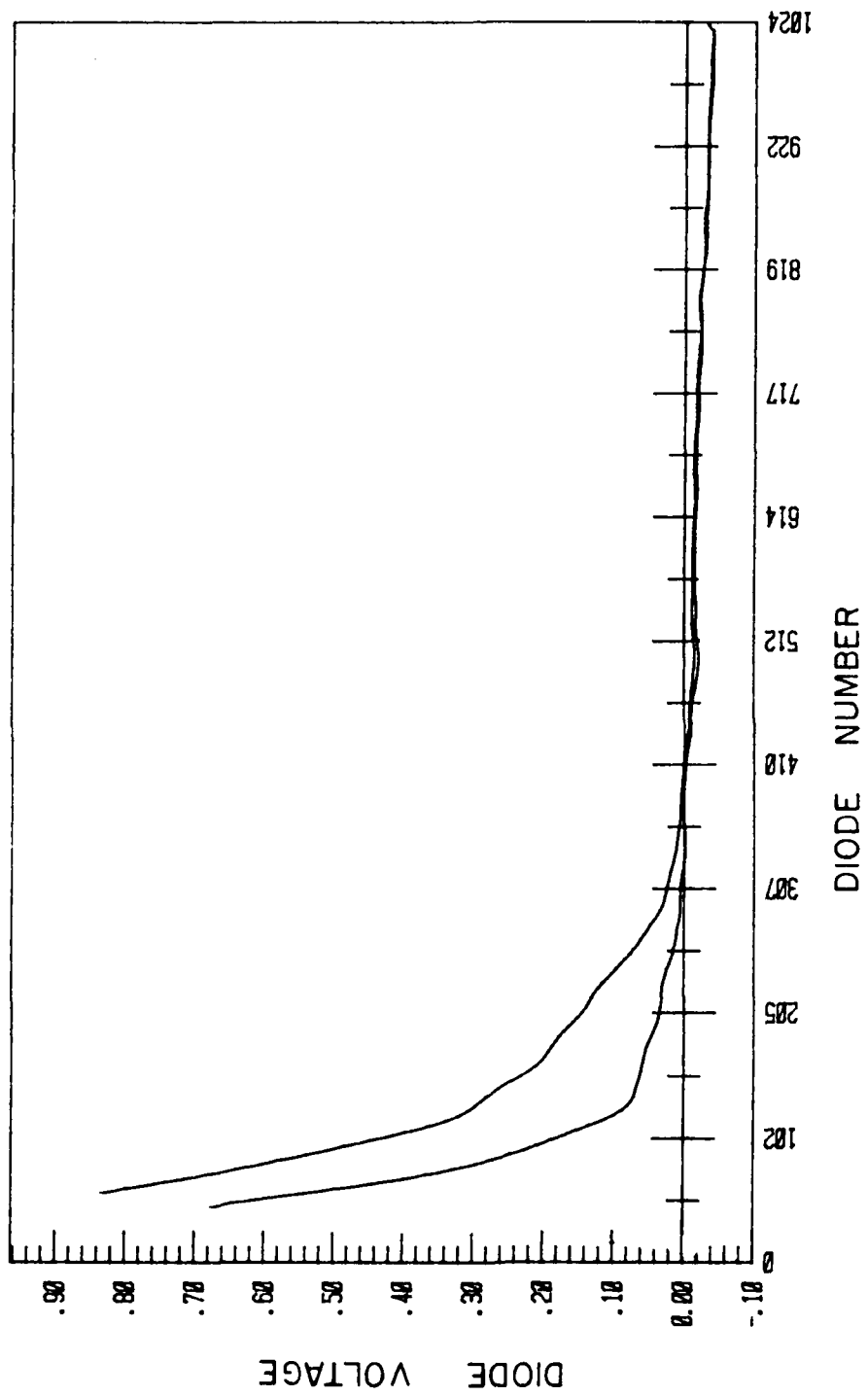


Figure 13. Voltage vs. Diode Number - 1 kHz Filter.

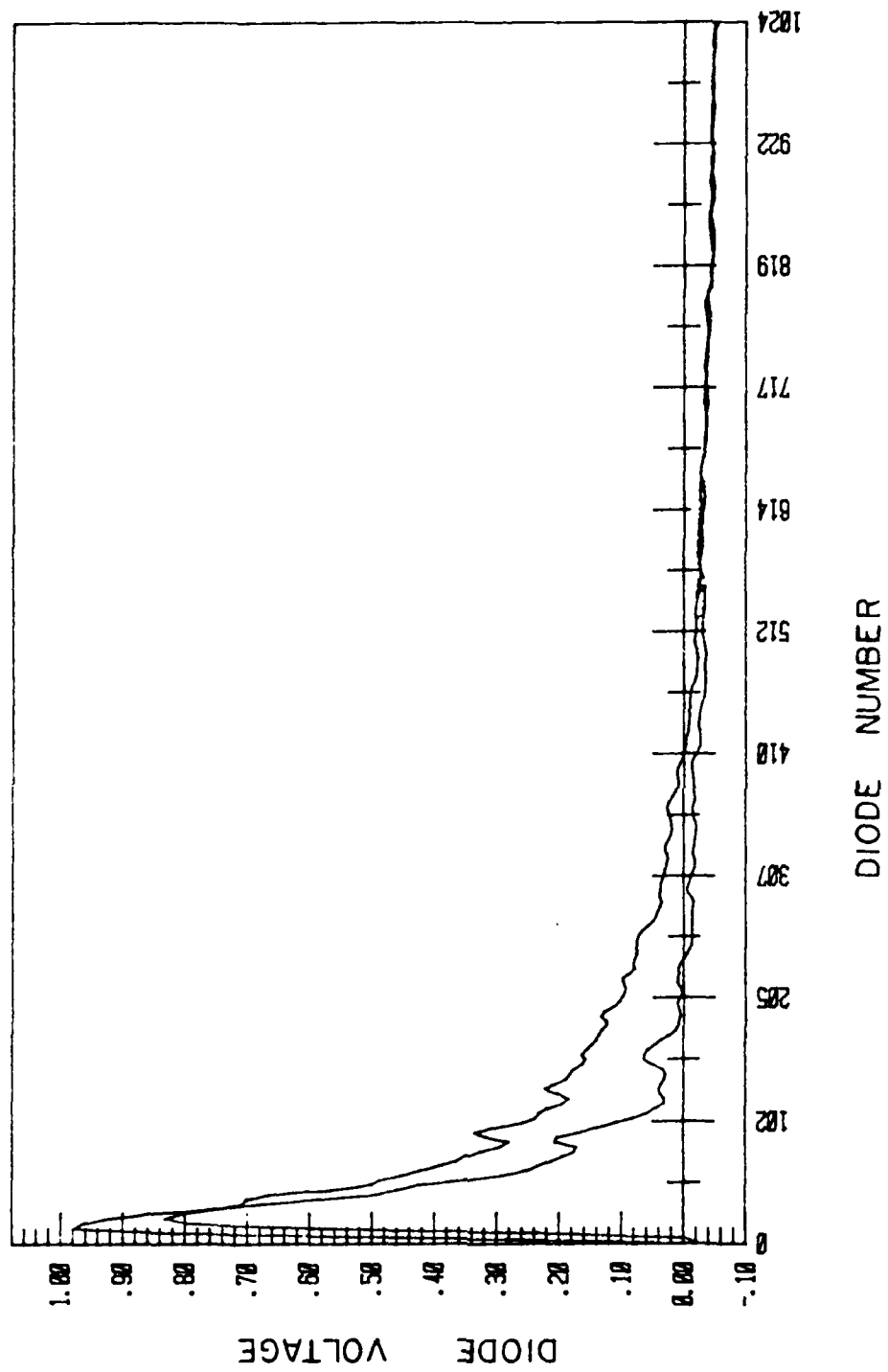


Figure 14. Voltage vs. Diode Number - 3 kHz Filter.

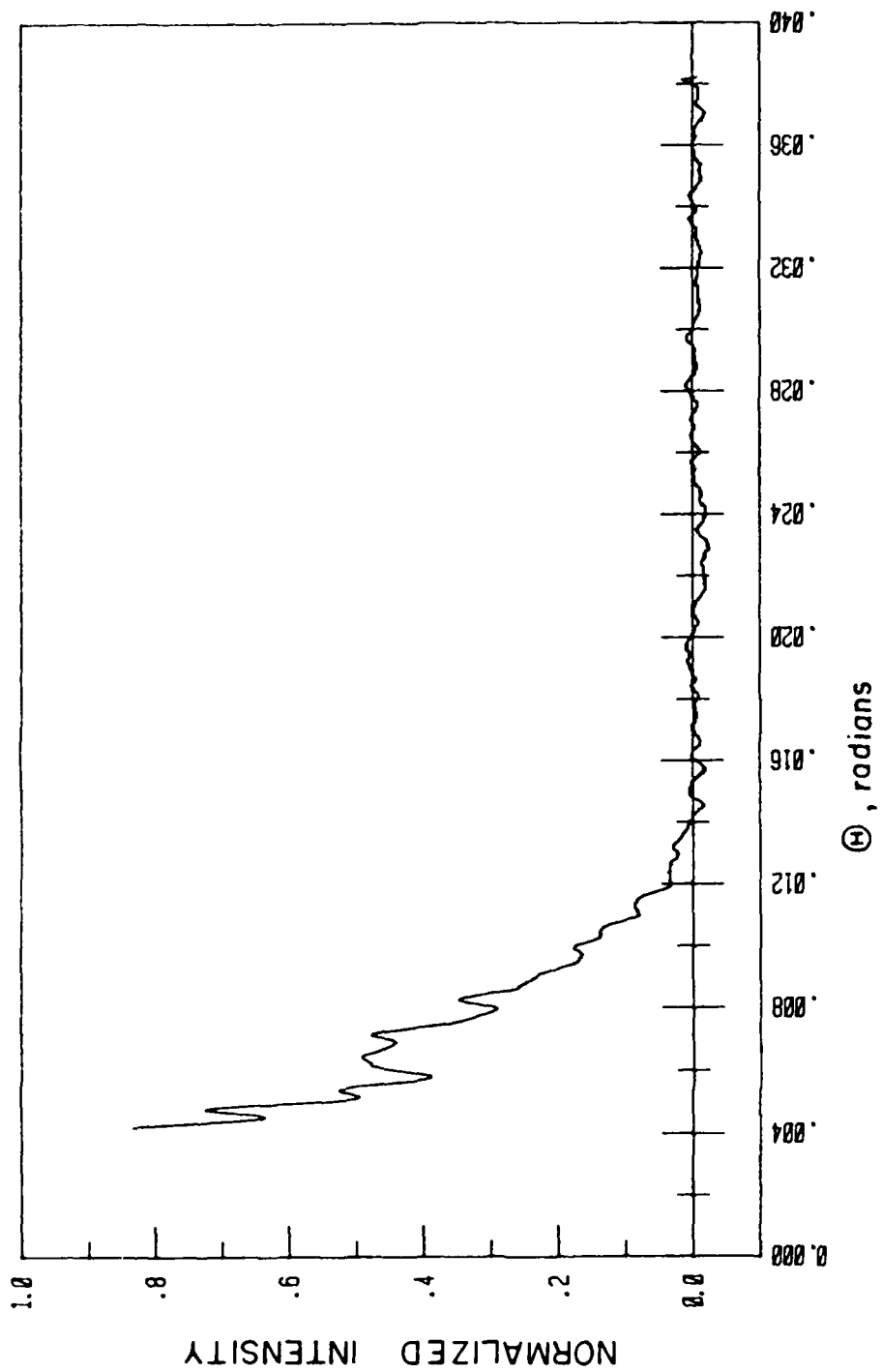


Figure 15. Example of Normalized Intensity vs. Scattering Angle Profile.

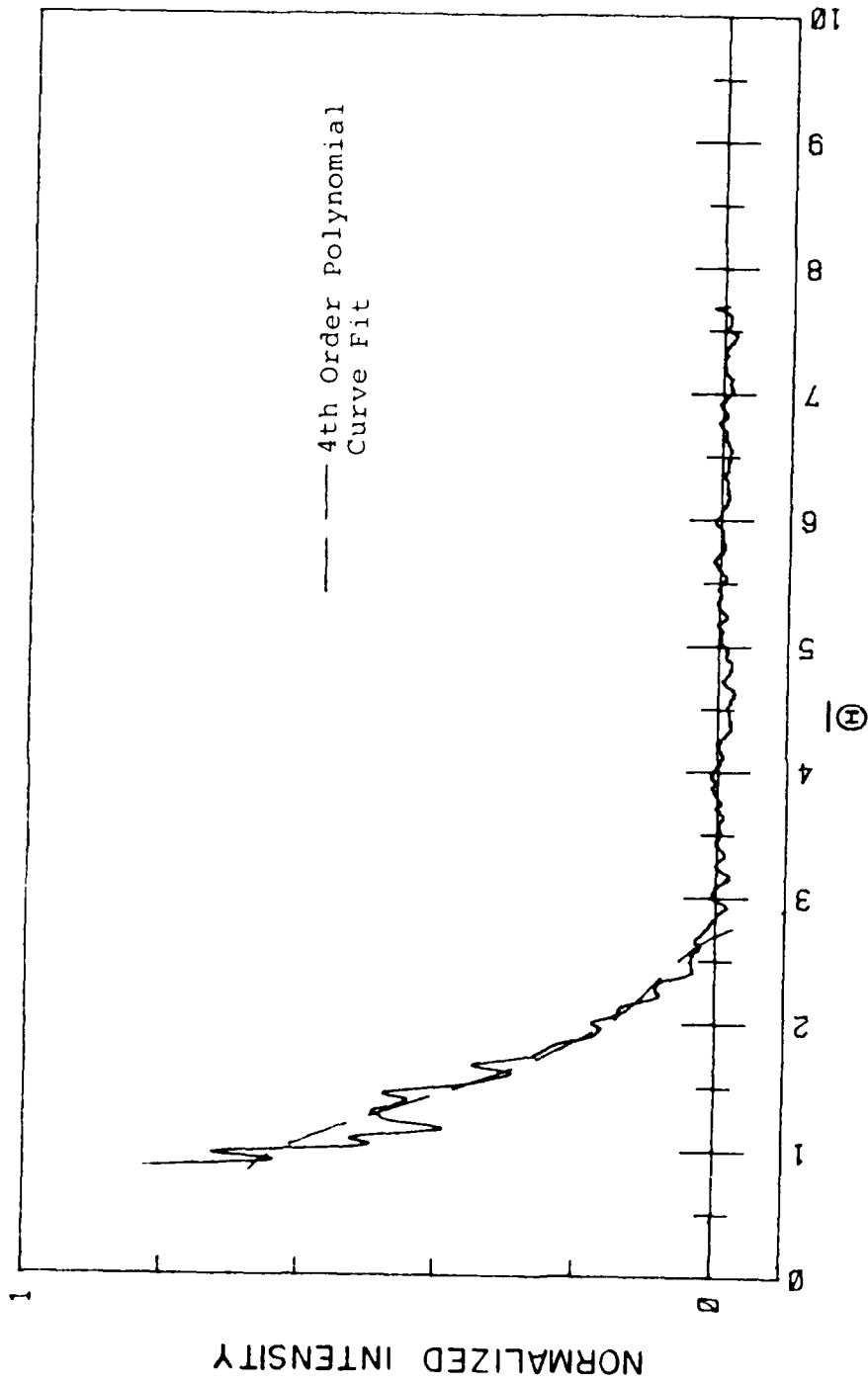


Figure 16. Example of Normalized Intensity vs. Dimensionless Scattering Angle Profile.

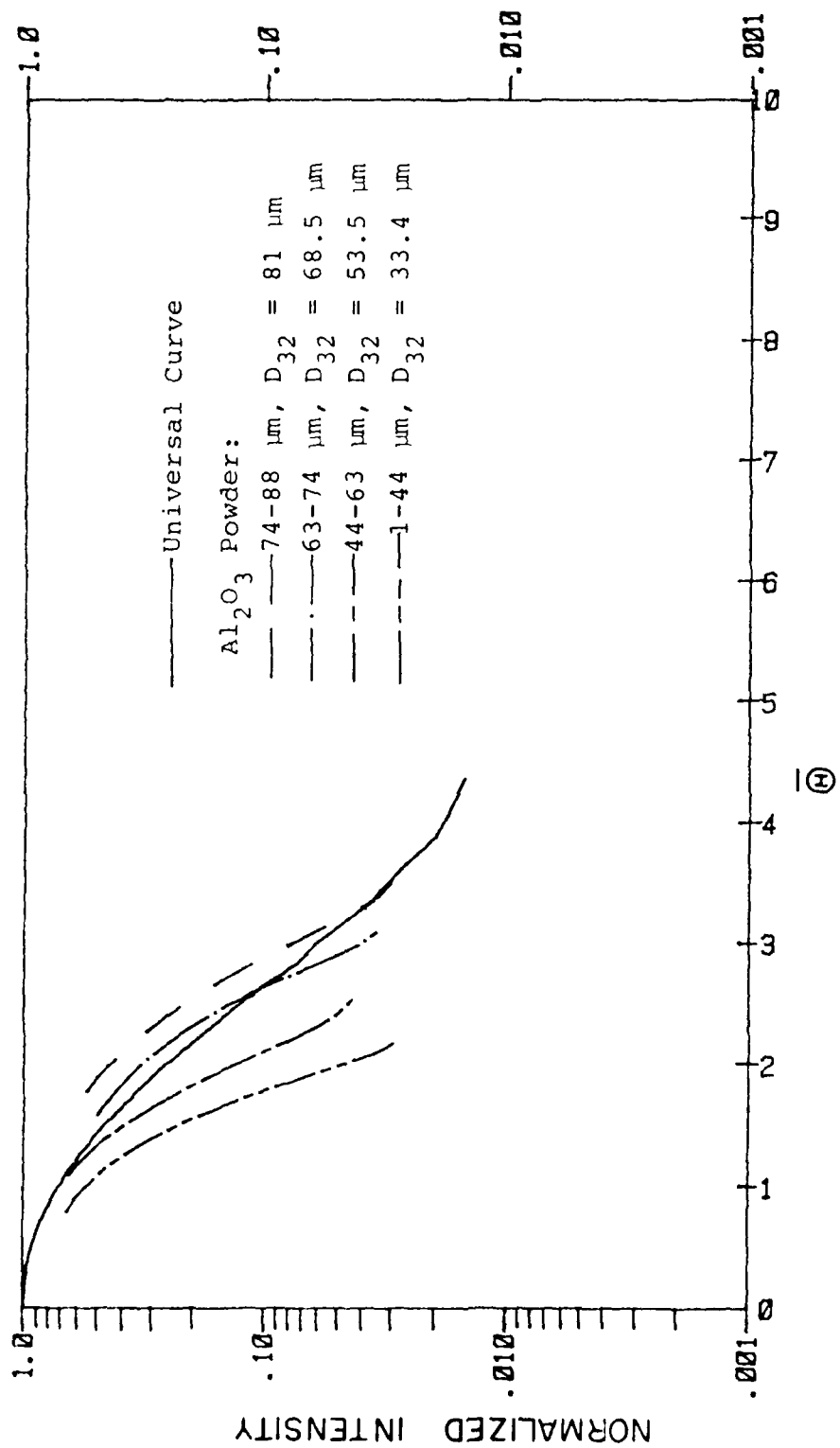


Figure 17. Normalized Intensity Profiles for Al<sub>2</sub>O<sub>3</sub> Powder.



Figure 18. SEM Photograph of Cleaned Exhaust Products.



Figure 19. SEM Photograph of Uncleaned Exhaust Products.

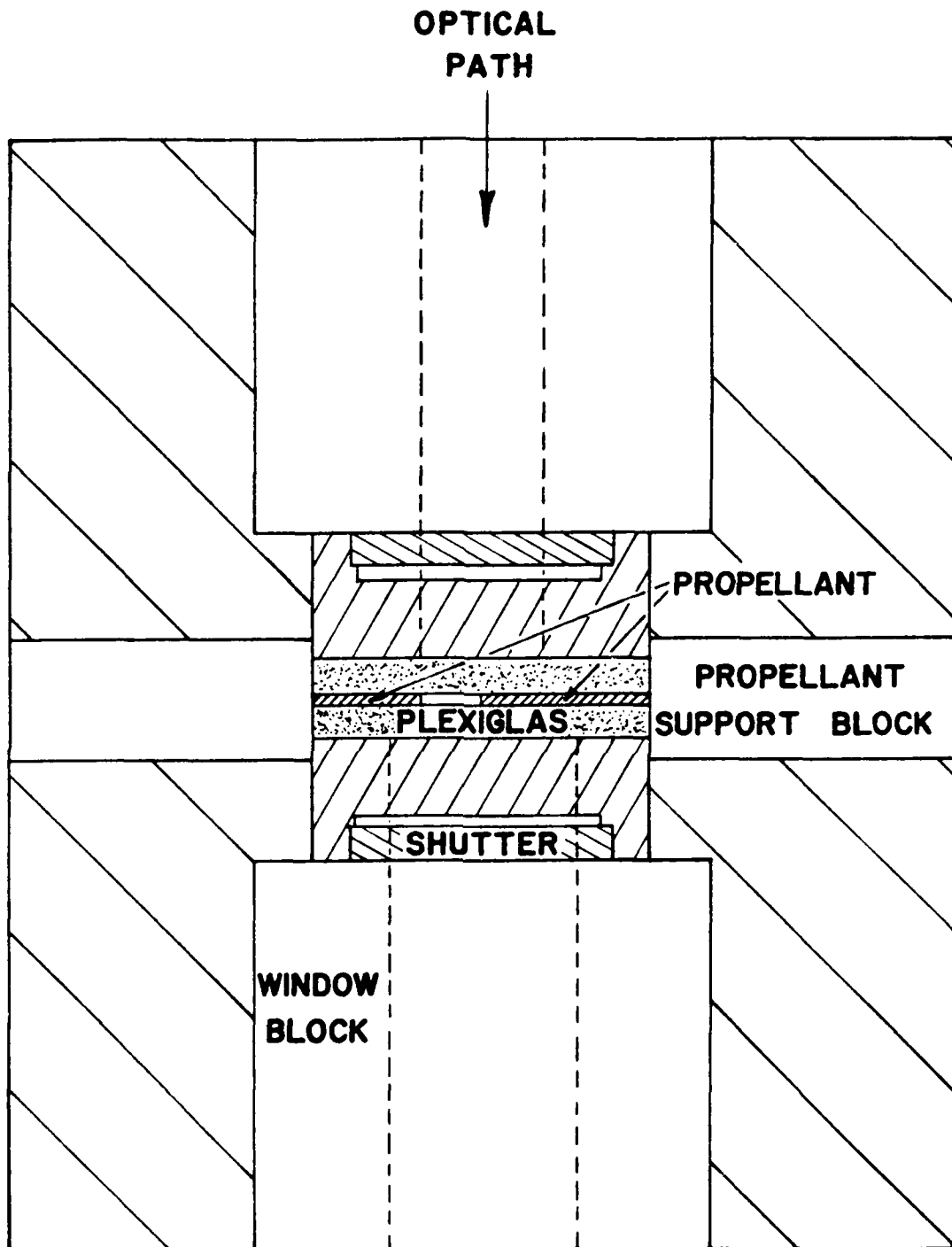


Figure 20. Initial 3-D Motor Configuration Showing Plexiglas Spacer Arrangement, Top View.

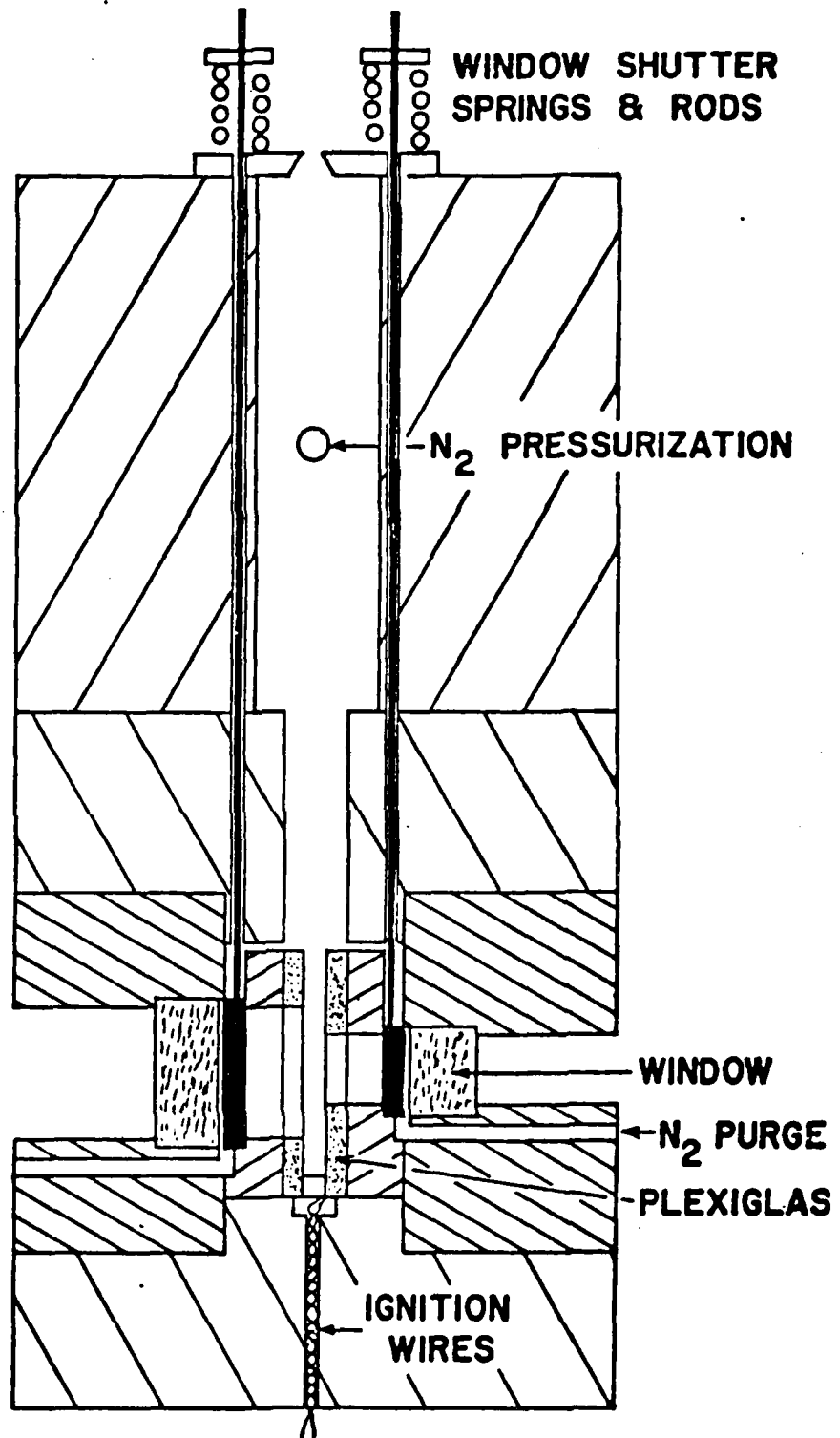


Figure 21. Initial 2-D Motor Configuration Showing Windows and Shutter Arrangement, Side View.

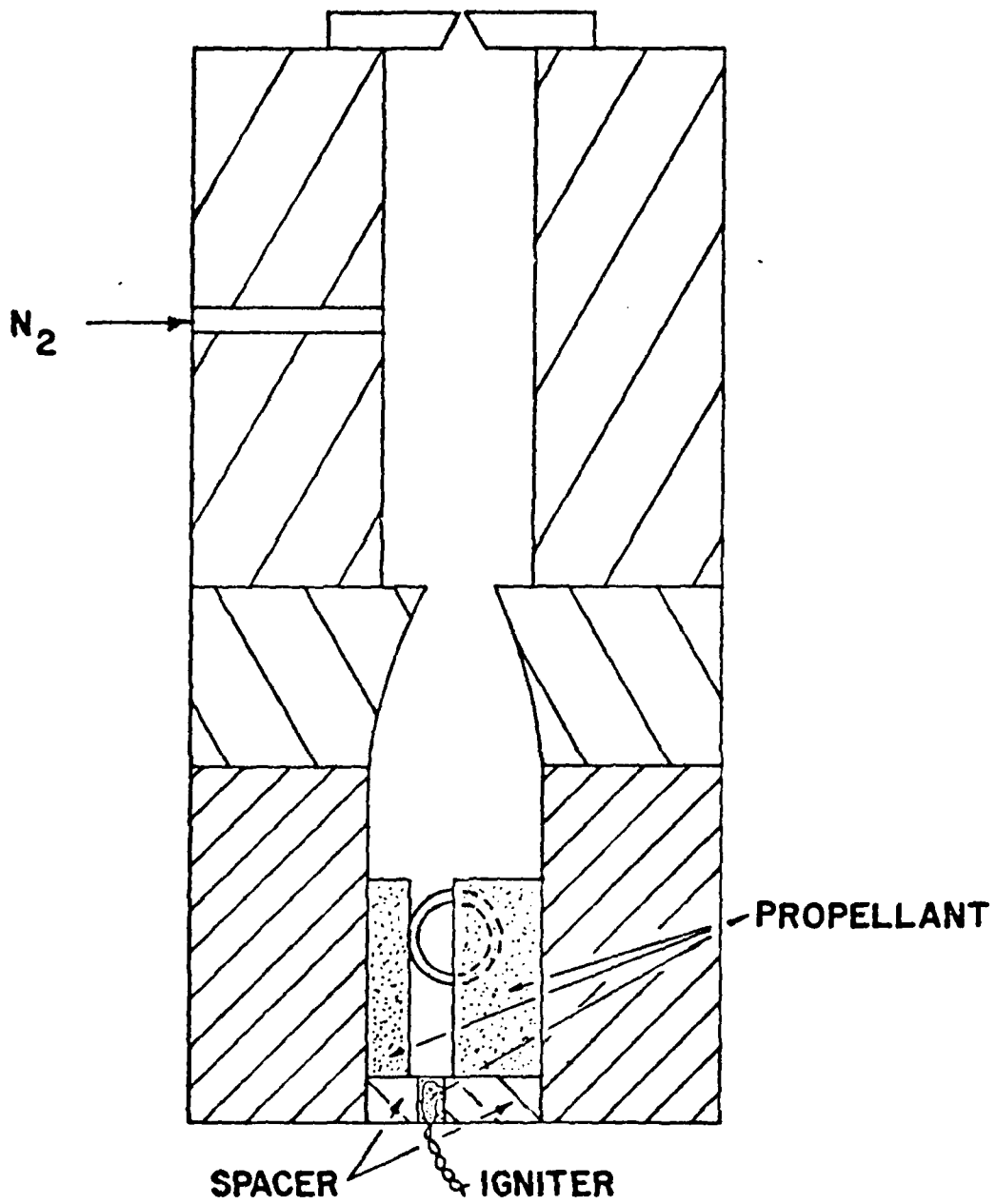


Figure 22. Initial 2-D Motor Configuration Showing Propellant Locations and Nitrogen Pressurization, Side View.

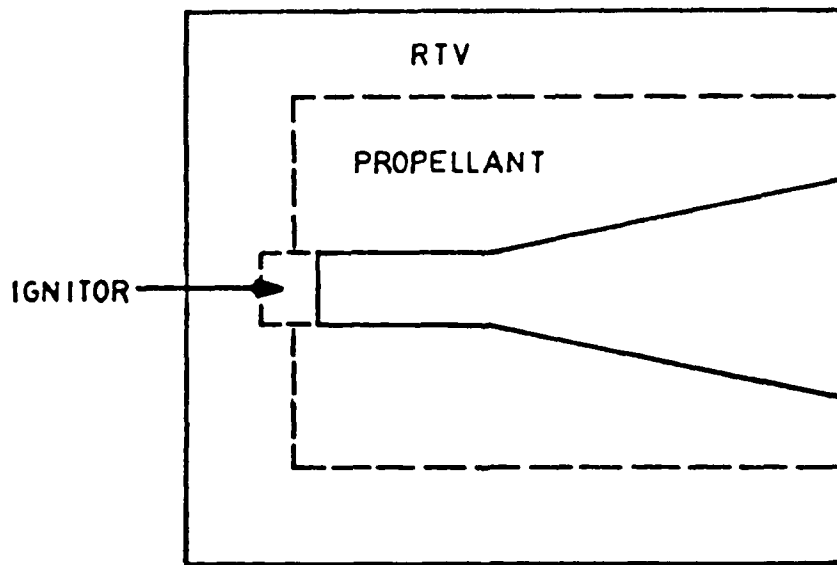
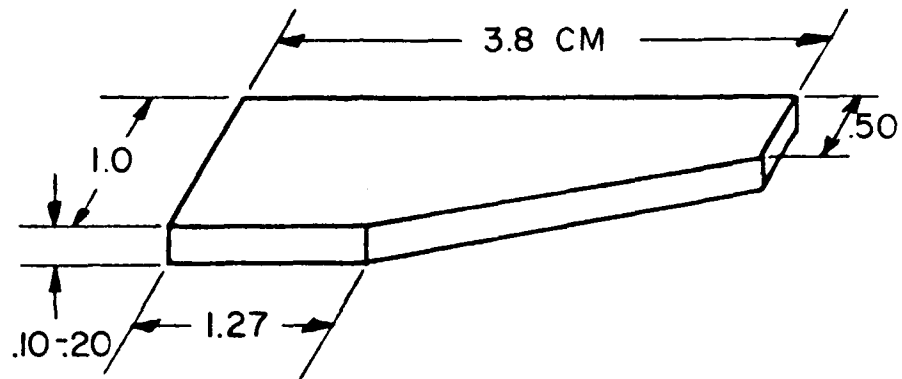


Figure 23. Propellant Slab Dimensions.

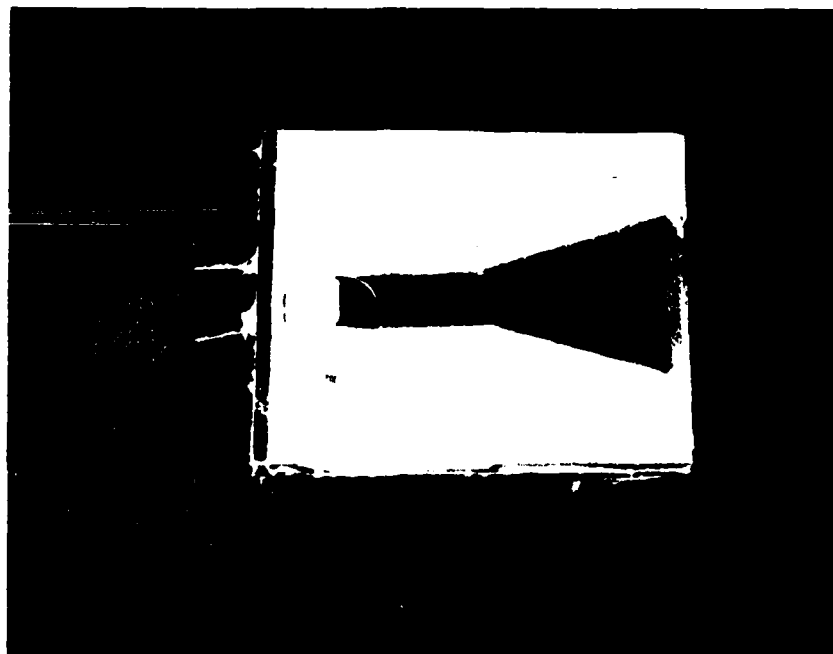


Figure 24. Propellant Mounted Between Glass Plates.

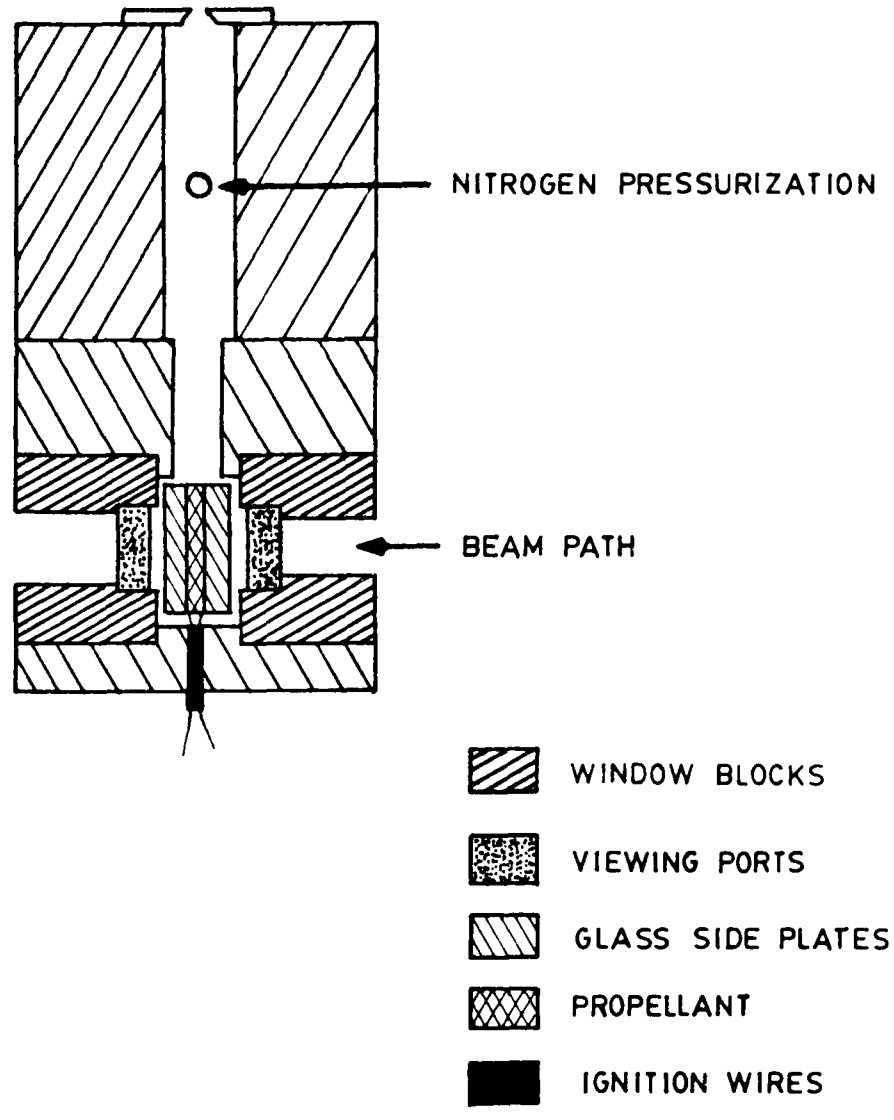


Figure 25. Schematic of 2-D Motor.

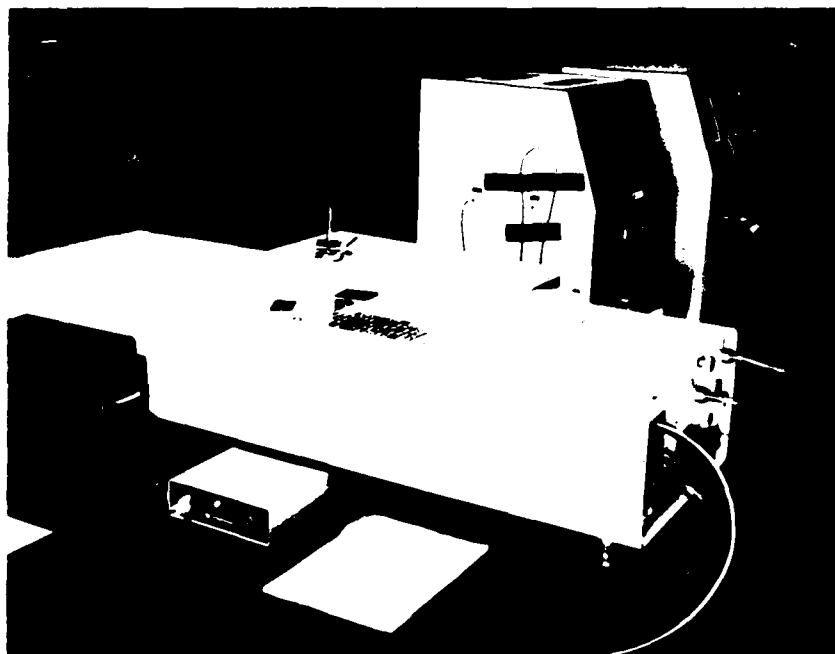


Figure 26. Q-Switched Pulsed Ruby Recording Laser.



Figure 27. Lens-Assisted Holographic System.



Figure 28. Holocamera Box.

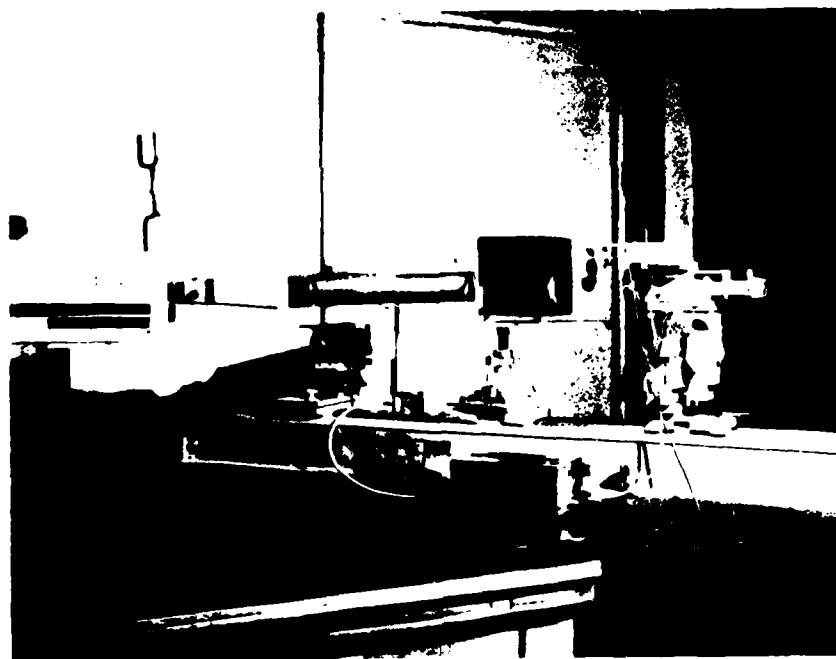


Figure 29. Holographic Reconstruction Apparatus.



Figure 30. Photograph of 0-80 Screw from Reconstructed Hologram.

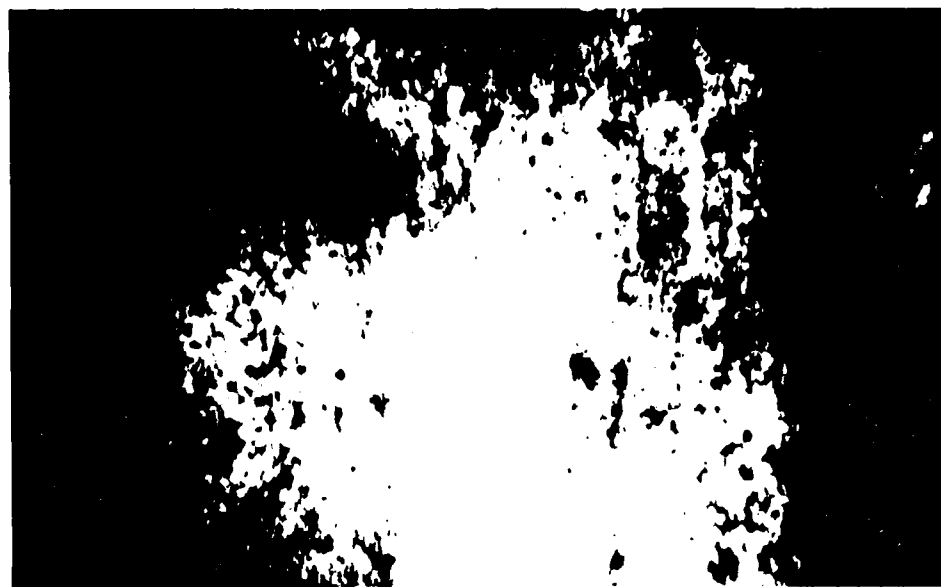


Figure 31. Photograph of Reconstructed Hologram of WGS-7A Burned at 26.5 atm, 1.2 mm Thick Slide Glass.



Figure 32. Photograph of Reconstructed Hologram of WGS-7A Burned at 41.8 atm, 5.6 mm Thick Borosilicate Glass.

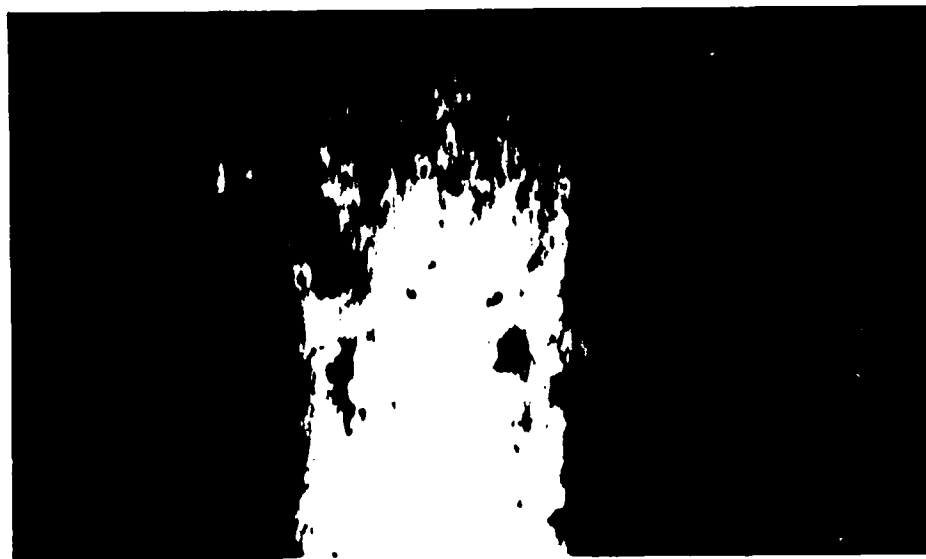


Figure 33. Photograph of Reconstructed Hologram of WGS-7A Burned at 34.0 atm, 5.6 mm Thick Borosilicate Glass.



Figure 34. Photograph of Reconstructed Hologram of WGS-6A Burned at 39.1 atm, 5.6 mm Thick Borosilicate Glass.

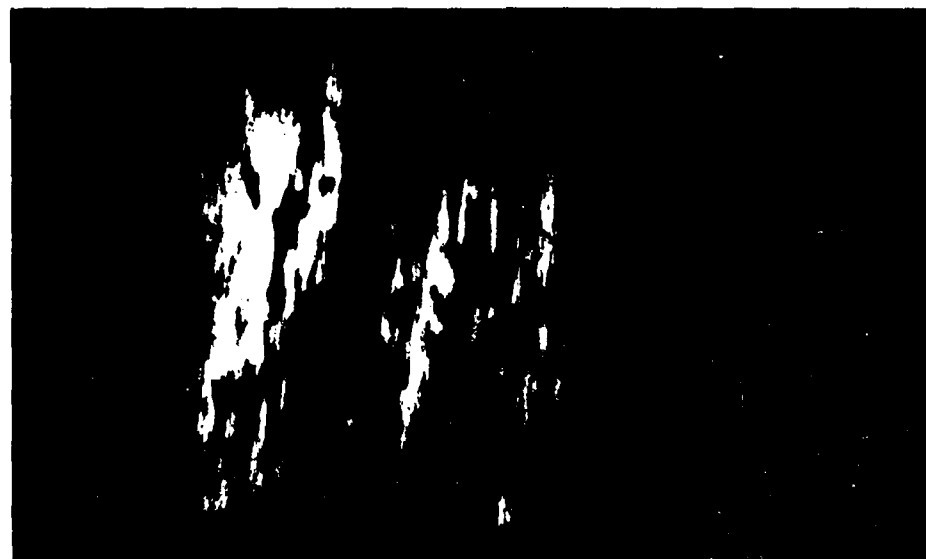


Figure 35. Photograph of Reconstructed Hologram of WGS-5A Burned at 36.4 atm, 5.6 mm Thick Borosilicate Glass.

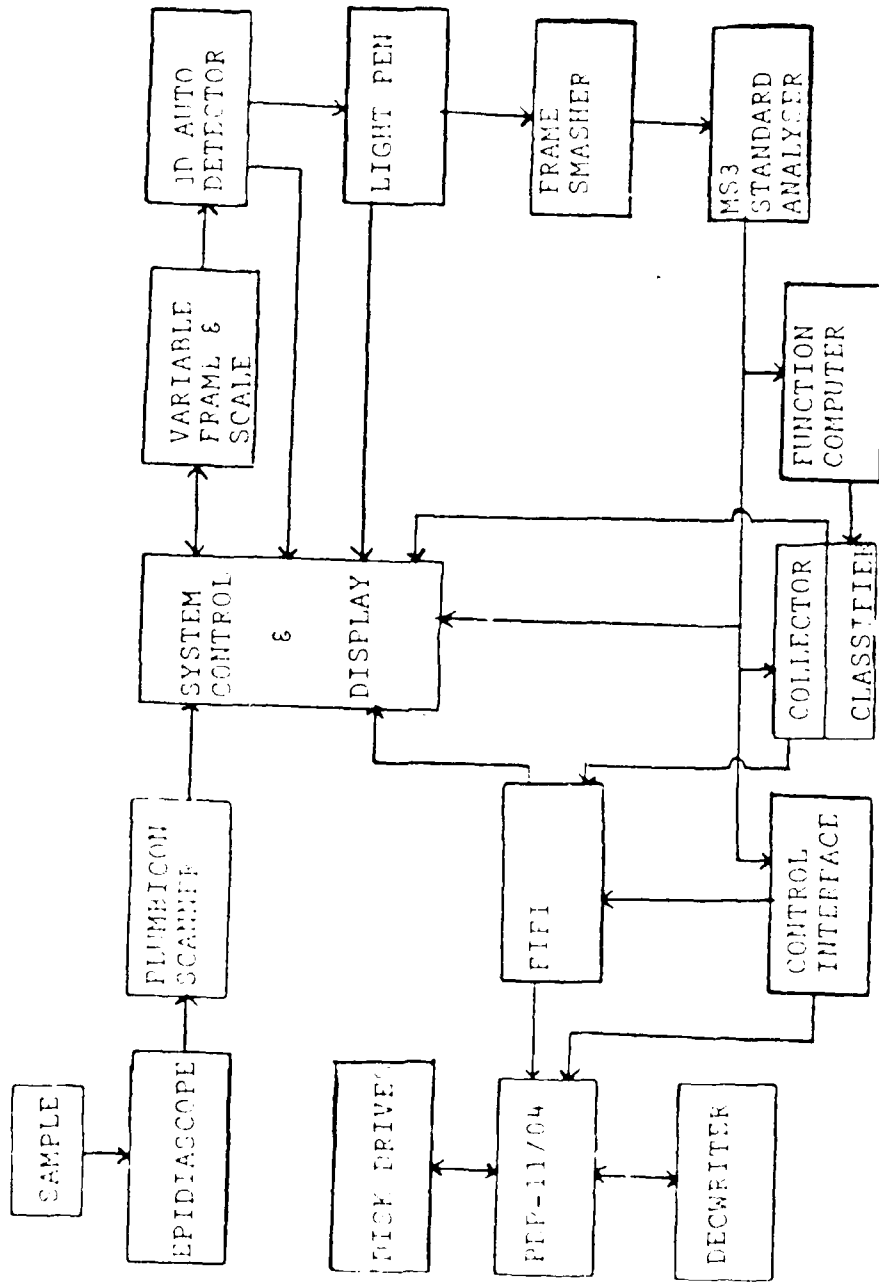


Figure 36. Block Diagram of Quantimet 720, Advanced Configuration.

AD-A141 044

AN INVESTIGATION OF EXPERIMENTAL TECHNIQUES FOR  
OBTAINING PARTICULATE BEH. (U) AIR FORCE ROCKET  
PROPULSION LAB EDWARDS AFB CA R G CRAMER ET AL. FEB 84

2/2

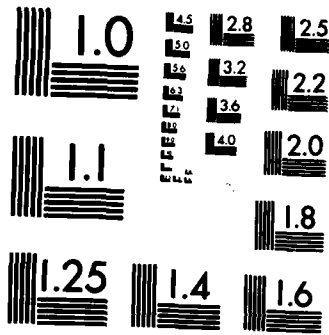
UNCLASSIFIED

AFRPL-TR-84-014 F04611-82-X-0008

F/G 21/9. 2

NL





MICROCOPY RESOLUTION TEST CHART  
NATIONAL BUREAU OF STANDARDS-1963-A

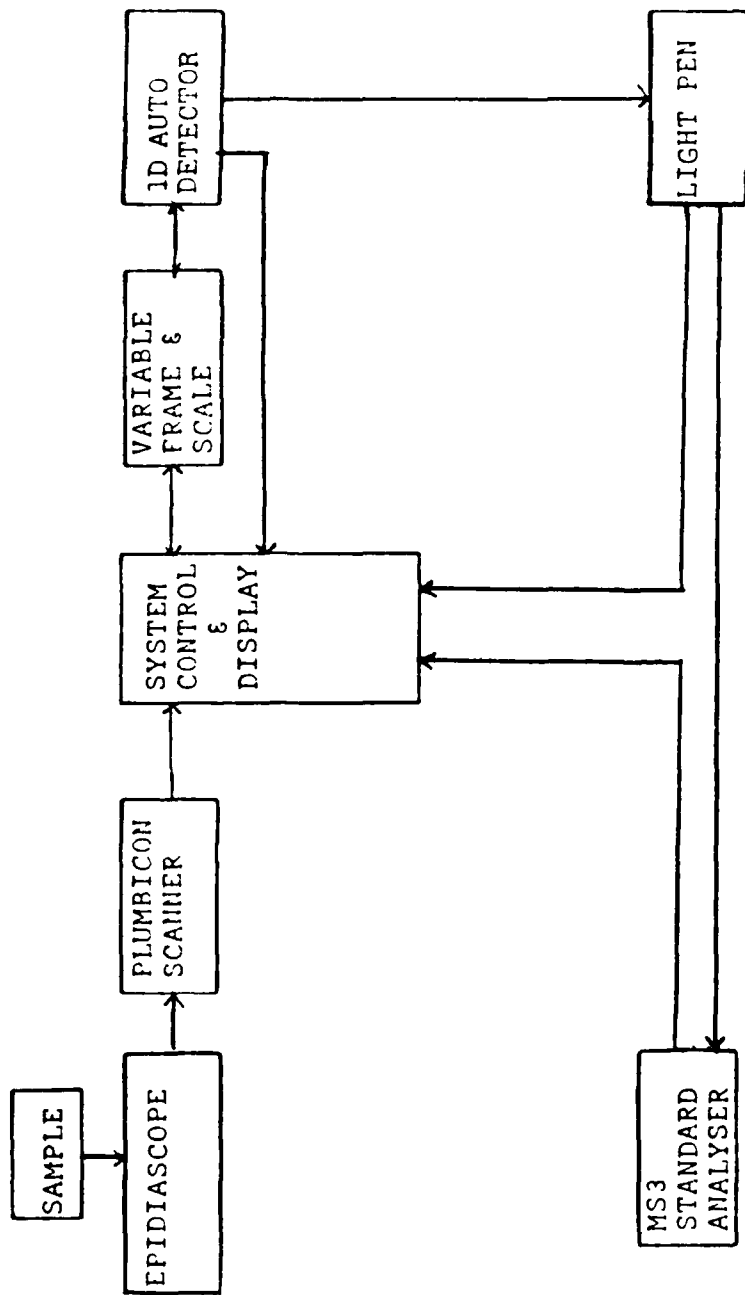


Figure 37. Block Diagram of Quantimet 720, Basic Configuration.

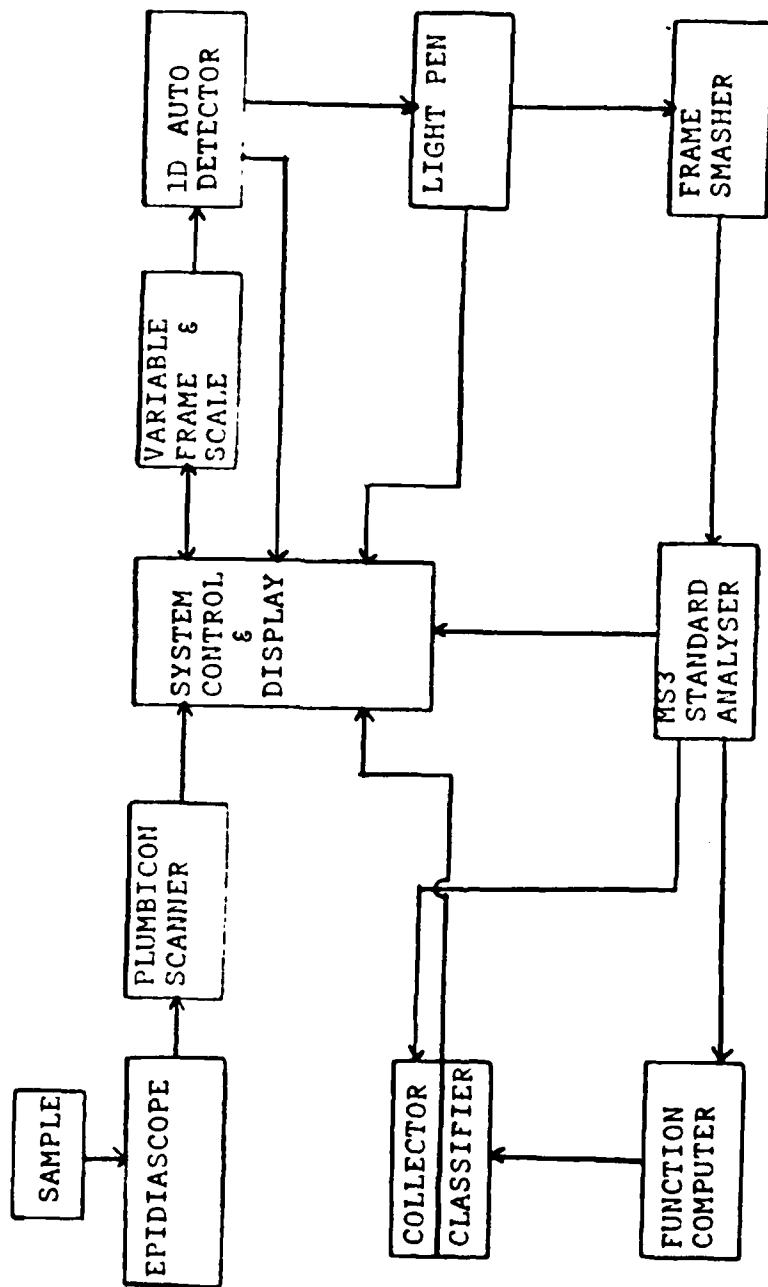


Figure 38. Block Diagram of Quantimet 720, Enhanced Basic Configuration.

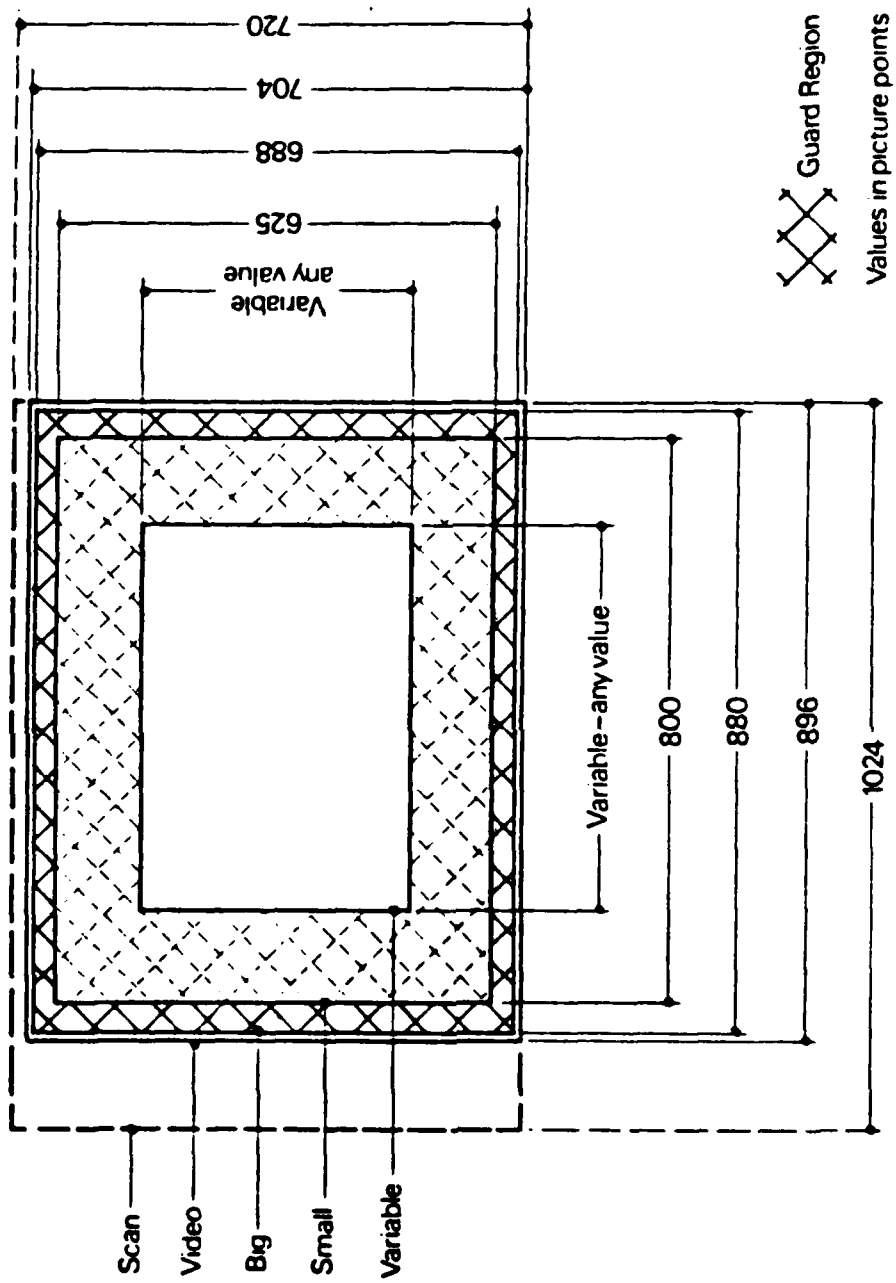


Figure 39. Frames Available in Quantimet 720.

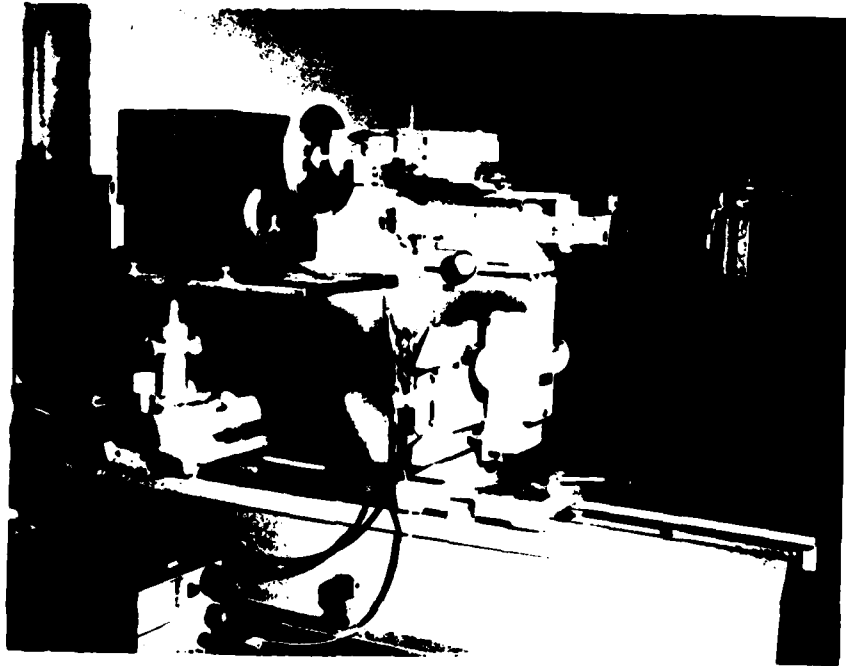


Figure 40. Setup for Photographing Holograms.

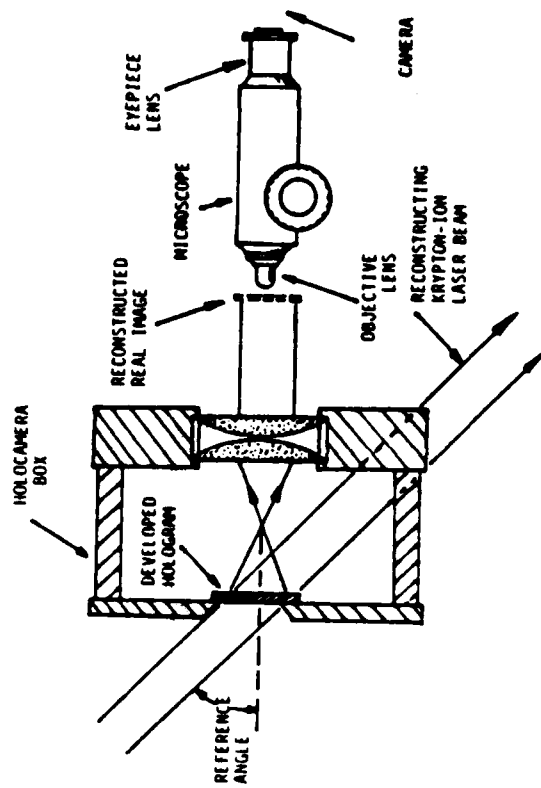


Figure 41. Schematic of Reconstruction and Viewing Method (Ref. 15).

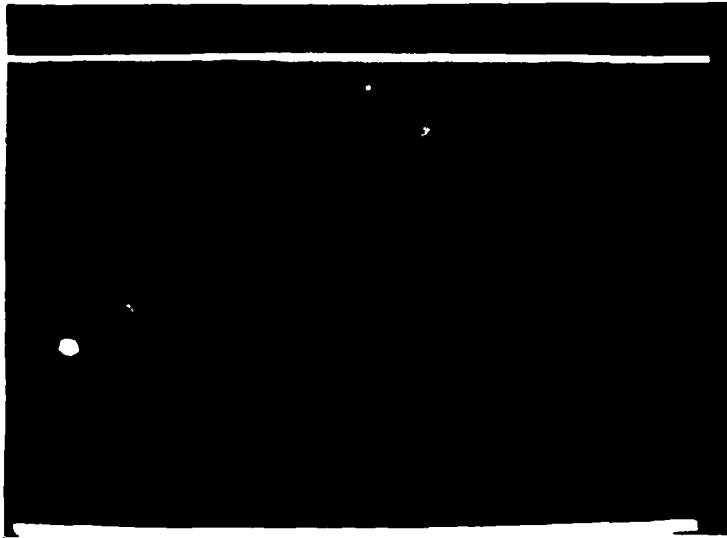


Figure 42. Photograph of Reconstructed Hologram of Propellant WGS-ZrC Burned at 36 atm.



Figure 43. Photograph of Reconstructed Hologram of Propellant WGS-ZrC Burned at 36 atm. Detected Region.

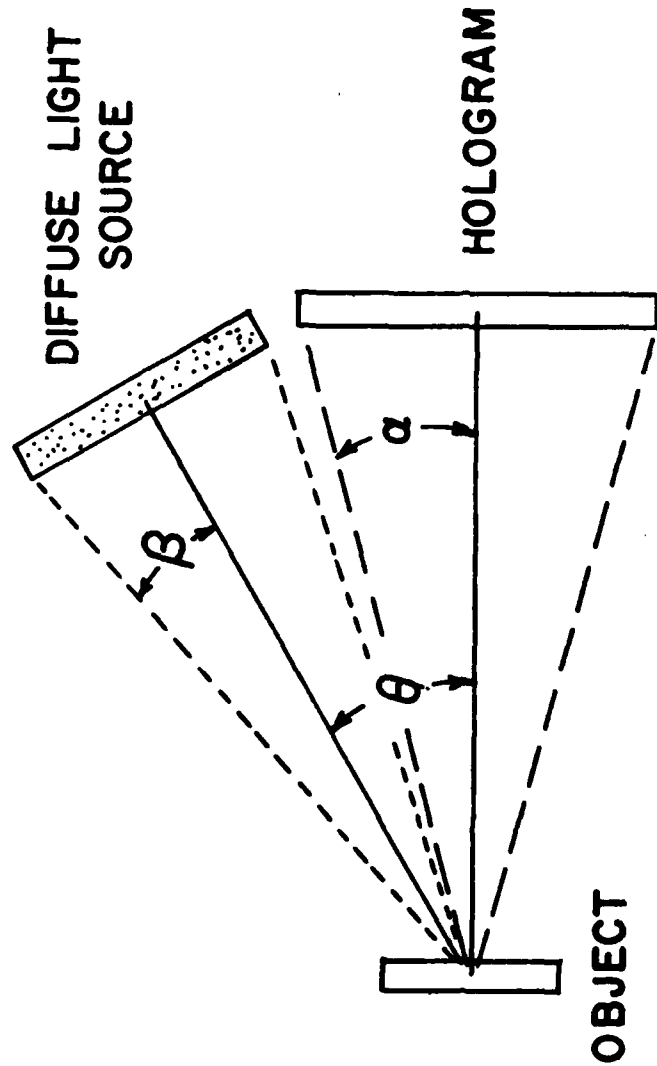


Figure 44. Geometry for Calculation of Speckle Diameter.

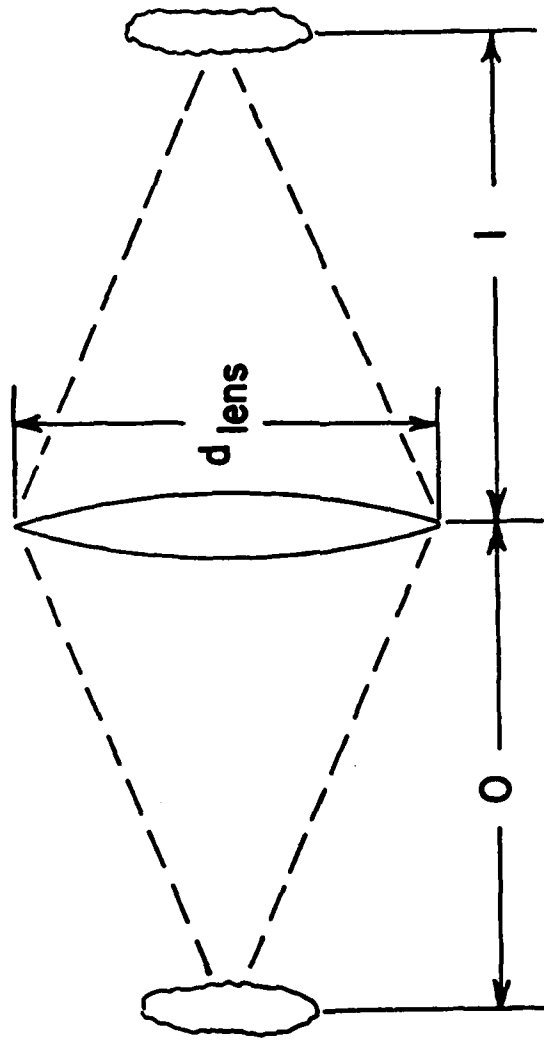


Figure 45. Imaging Lens Geometry.

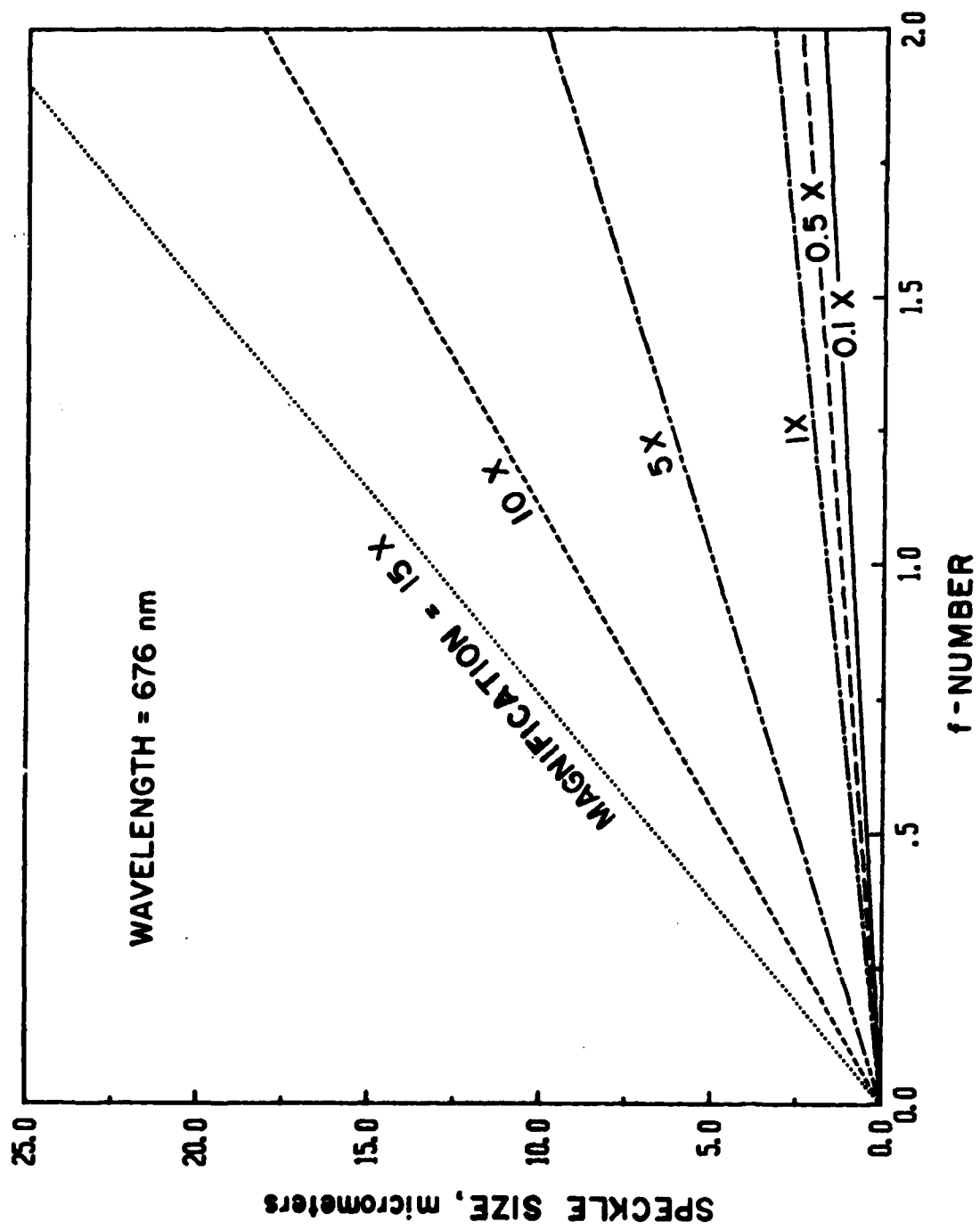
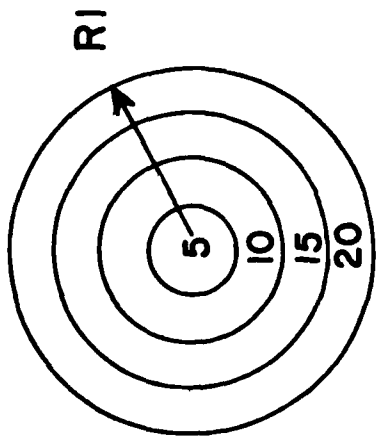
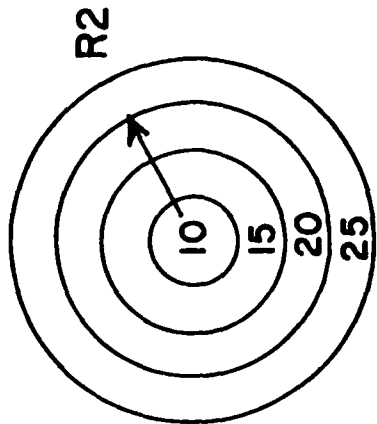


Figure 46. Speckle Size vs. Lens f-Number and Magnification.



LOW ILLUMINATION



HIGH ILLUMINATION

Figure 47. Grey Level Map of Two Differently Illuminated, Equally-Sized, Particles.

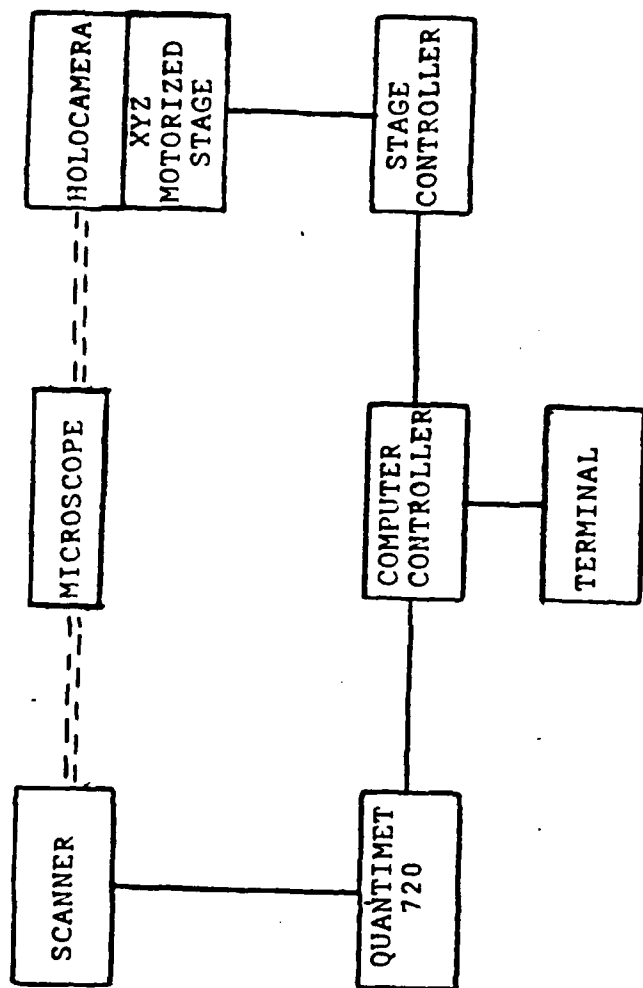


Figure 48. Semiautomatic Quantimet 720 Block Diagram.

REPROD

FILMED

ENDING

